NATIONAL
OPTICAL
ASTRONOMY
OBSERVATORIES

Preprint Series

NOAO Preprint No. 813

WFPC2 OBSERVATIONS OF STAR CLUSTERS IN THE MAGELLANIC CLOUDS. II. THE OLDEST STAR CLUSTERS IN THE SMALL MAGELLANIC CLOUD

Kenneth J. Mighell
Ata Sarajedini
Rica S. French

To appear in: The Astronomical Journal

August 1998

Operated for the National Science Foundation by the Association of Universities for Research in Astronomy, Inc.

To appear in the Astronomical Journal (accepted 1998 August 10)

WFPC2 OBSERVATIONS OF STAR CLUSTERS IN THE MAGELLANIC CLOUDS. II. THE OLDEST STAR CLUSTERS IN THE SMALL MAGELLANIC CLOUD[1]

KENNETH J. MIGHELL[2]
Kitt Peak National Observatory, National Optical Astronomy Observatories[3],
P. O. Box 26732, Tucson, AZ 85726-6732
Electronic mail: mighell@noao.edu

ATA SARAJEDINI[4]
Department of Physics and Astronomy, San Francisco State University, 1600 Holloway Avenue, San Francisco, CA 94132
Electronic mail: ata@stars.sfsu.edu

RICA S. FRENCH[5]
Middle Tennessee State University, Physics & Astronomy Department, WPS 219, P. O. Box 71, Murfreesboro, TN 37132
Electronic mail: sirbaugh@physics.mtsu.edu

---

[1]Based on observations made with the NASA/ESA *Hubble Space Telescope*, obtained from the data archive at the Space Telescope Science Institute, which is operated by the Association of Universities for Research in Astronomy, Inc. under NASA contract NAS5-26555.

[2]Guest User, Canadian Astronomy Data Centre, which is operated by the Dominion Astrophysical Observatory for the National Research Council of Canada's Herzberg Institute of Astrophysics.

[3]NOAO is operated by the Association of Universities for Research in Astronomy, Inc., under cooperative agreement with the National Science Foundation.

[4]Hubble Fellow

[5]Based on research conducted at NOAO as part of the Research Experiences for Undergraduates program.

ABSTRACT

We present our analysis of archival *Hubble Space Telescope* Wide Field Planetary Camera 2 (WFPC2) observations in F450W ($\sim B$) and F555W ($\sim V$) of the intermediate-age populous star clusters NGC 121, NGC 339, NGC 361, NGC 416, and Kron 3 in the Small Magellanic Cloud. We use published photometry of two other SMC populous star clusters, Lindsay 1 and Lindsay 113, to investigate the age sequence of these seven populous star clusters in order to improve our understanding of the formation chronology of the SMC. We analyzed the V vs $B-V$ and M_V vs $(B-V)_o$ color-magnitude diagrams of these populous Small Magellanic Cloud star clusters using a variety of techniques and determined their ages, metallicities, and reddenings. These new data enable us to improve the age-metallicity relation of star clusters in the Small Magellanic Cloud. In particular, we find that a closed-box continuous star-formation model does not reproduce the age-metallicity relation adequately. However, a theoretical model punctuated by bursts of star formation is in better agreement with the observational data presented herein.

Subject headings: galaxies: clusters: individual (Kron 3, Lindsay 1, Lindsay 113, NGC 121, NGC 339, NGC 361, NGC 416) — galaxies: evolution — galaxies: individual (Small Magellanic Cloud) — galaxies: star clusters — Local Group

1. INTRODUCTION

We can improve our understanding of the early chemical enrichment history of the Small Magellanic Cloud (SMC) by investigating the ages and abundances of its oldest star clusters. A recent summary of the SMC age-metallicity relation may be found in Fig. 1a of the review article by Olszewski, Suntzeff, & Mateo (1996). In an earlier review article, Da Costa (1991) notes that the most metal-poor clusters in the SMC have similar metallicities yet apparently very different ages indicating that this galaxy has had an unusual chemical enrichment history. The major caveat to this conclusion was that the observational errors were large; typical error bars in [Fe/H] were between ± 0.2 and ± 0.4 dex while the age errors were between ± 2 and ± 3 Gyr. This has lead to significant uncertainty in our present understanding of the age-metallicity relationship for the SMC.

It has only recently been established that the most metal poor globular clusters in the Large Magellanic Cloud (LMC) have ages that are comparable to the ages of the metal-poor Galactic globular clusters (Hodge 11: Mighell *et al.* 1996; NGC 1786, 1841, 2210: Brocato *et al.* 1996; NGC 1754, 1835, 1898, 2005, 2109: Olsen *et al.* 1998). The populous LMC star cluster ESO 121-SC03 has an age of $\sim$9 Gyr and is the only intermediate-age star cluster in the LMC within the age

range of 3 and 12 Gyr (Geisler *et al.* 1997, and references therein). Recent work suggests that ESO 121-SC03 may not be alone (Sarajedini 1998).

The SMC has at least 7 populous star clusters that are metal-poor ([Fe/H] $\lesssim -1.0$) with ages between $\sim$5 and $\sim$12 Gyr: Lindsay 113, Kron 3, NGC 339, NGC 416, NGC 361, Lindsay 1, NGC 121. All these populous clusters have similar metallicities and horizontal branch (HB) morphologies that are predominantly redward of the RR Lyrae instability strip. In our recent investigation of three SMC intermediate-age populous clusters (NGC 416, Lindsay 1, Lindsay 113) we showed how existing SMC cluster ages in the literature derived from integrated photometry can be very unreliable (Mighell, Sarajedini, & French 1998; hereafter PAPERI). Geisler *et al.* (1997) found similar problems with published LMC cluster ages derived from integrated photometry. The unintended inclusion of bright field main-sequence stars and the poor age sensitivity provided by broad-band colors for star clusters older than a few Gyr are the two principle reasons why integrated cluster photometry can confuse intermediate-age clusters with genuine old clusters.

The more massive LMC has received considerably more attention by stellar population researchers than has the SMC. The early photographic studies of NGC 361 (Arp 1958) and NGC 339 (Gascoigne 1966) have the only color-magnitude diagrams of these SMC clusters available in the refereed literature. Most of the clusters that do have CCD-based color-magnitude diagrams are from studies that used early CCD cameras in the 1980's. Modern cluster observations using large-format low-noise CCDs can significantly improve our knowledge of the oldest star clusters in the Small Magellanic Cloud. The analysis of color-magnitude diagrams produced from such studies can provide cluster age and metallicity data which complements and enhances chemical abundance studies based on spectroscopic observations of cluster red giants (e.g., Da Costa & Hatzidimitriou 1998, hereafter DH98).

In this work, we improve our understanding of the early chemical enrichment history of the Small Magellanic Cloud using archival WFPC2 data and previously published photometry of its oldest star clusters. Section 2 is a discussion of the observations and photometric reductions. We present our color-magnitude diagrams of the SMC star clusters NGC 416, NGC 121, NGC 339, NGC 361, and Kron 3 in Sec. 3. We estimate the reddenings and metallicites of the oldest SMC star clusters in Sec. 4 and estimate their ages in Sec. 5. Section 6 is a discussion of the early star formation history of the SMC galaxy. We then present our conclusions and thoughts about future studies of the stellar populations of the Small Magellanic Cloud in the final section of this paper.

2. OBSERVATIONS AND PHOTOMETRIC REDUCTIONS

The SMC populous star clusters NGC 121, NGC 339, NGC 361, NGC 416, and Kron 3 were observed with the *Hubble Space Telescope* Wide Field Planetary Camera 2 (WFPC2) between 1994 January 26 and 1994 May 27 through the F450W ($\sim B$) and F555W ($\sim V$) filters. The WFPC2 PC1 aperture (Biretta *et al.* 1996) was centered on the target positions given in Table

1 and shown in Fig. 1. Ten high-gain observations were obtained. These WFPC2 datasets were recalibrated at the Canadian Astronomy Data Centre and retrieved electronically by us using a guest account which was kindly established for KJM. •TAB1 •FIG1

The data were analyzed with the CCDCAP[6] digital circular aperture photometry code developed by Mighell to analyze *HST* WFPC2 observations. We followed the same WFPC2 data reduction procedures of Mighell (1997) except for the following details. A fixed aperture with a radius of 2.0 pixels was used for all stars on the WFPC2 CCDs. The local background level was determined from a robust estimate of the mean intensity value of all pixels between 2.0 and 5.5 pixels from the center of the circular stellar aperture. The Charge Transfer Effect was removed from the instrumental magnitudes by using a 4% uniform wedge along the Y-axis of each CCD as described in Holtzman *et al.* (1995a). We used the standard WFPC2 magnitude system (Holtzman *et al.* 1995a) which is defined using 1″ diameter apertures containing about 90% of the total flux from a star. The instrumental magnitudes, b_r and v_r, were transformed to Johnson B and V magnitudes using the following equations $B = b_r + \Delta_r + \delta_r + [0.230\pm0.006](B-V) + [-0.003\pm0.006](B-V)^2 + [21.175\pm0.002]$ and $V = v_r + \Delta_r + \delta_r + [-0.060\pm0.006](B-V) + [0.033\pm0.002](B-V)^2 + [21.725\pm0.004]$ where an instrumental magnitude of zero is defined as one DN/sec at the high gain state ($\sim$14 e^-/DN). The constants come from Tables 10 and 7, respectively, of Holtzman *et al.* (1995a). These color equations were used by Mighell *et al.* (1996) to show that the age of Large Magellanic Cloud cluster Hodge 11 is identical to that of the Galactic globular cluster M92 with a relative age-difference uncertainty ranging from 10% to 21%. The values for average aperture corrections, $\langle\Delta_r\rangle$, are listed in Table 2. The zero-order ("breathing") aperture corrections for these observations (δ_r : see Table 3) were computed using a large aperture with a radius of 3.0 pixels and a background annulus of $3.0 \leq r_{\rm sky} \leq 6.5$ pixels. •TAB2 •TAB3

Most of these observations were obtained when the WFPC2 CCDs operated at a temperture of −76 °C (the standard CCD operating temperature before 1994 April 23). At this temperature, the number of "hot" pixels on a WFPC2 CCD would grow at a rate of several thousand pixels per month per chip (Holtzman *et al.* 1995b). There was a small but statistically significant position shift for stars between the F450W and F555W images. Hot pixels and other CCD defects did not exhibit this position shift. We took advantage of this fact to reject all point-source candidates with a position shift that were not within 2 average deviations of the median shift on each WFPC2 CCD. This procedure allowed us to statistically remove most of the hot pixels and other CCD defects.

We have used the standard Charge Transfer Effect correction (4% uniform wedge along the Y-axis of each CCD) recommended by Holtzman *et al.* (1995a) for all our observations regardless of the CCD operating temperature at which they were obtained. While Holtzman

[6]IRAF implementations of CCDCAP are now available over the Wide World Web at the following site: `http://www.noao.edu/noao/staff/mighell/ccdcap/`

et al. (1995a) consider −76 °C data to have larger uncertainties associated with CTE, we note that the application of the standard 4% CTE correction worked well in the Hodge 11 analysis of Mighell *et al.* (1996) whose V magnitude zeropoint differed from Walker's (1993) by a statisically insignificant 0.009 ± 0.010 mag. The Hodge 11 data analyzed by Mighell *et al.* (1996) was obtained on 1994 February 1; the use of a CTE correction of 12% used by Holtzman *et al.* (1995a) on their −76 °C data would have clearly resulted in worse photometry for the Hodge 11 observations.

We present our WFPC2 stellar photometry of stars found in NGC 416, NGC 121, NGC 339, NGC 361, and Kron 3 in Tables 4, 5, 6, 7, and 8, respectively. The first column gives the identification (ID) of the star. The left-most digit of the ID gives the WFPC2 chip number (1, 2, 3, or 4) where the star was found. The right-most 4 digits gives the x coordinate of the star multiplied by 10. The remaining 4 digits gives the y coordinate of the star multiplied by 10. For example, the first star in Table 4 has an ID of 106084534 which indicates that it has the (x, y) position of $(60.8, 453.4)$ on the PC1 CCD. The second and third columns give the V magnitude and its rms $(1\,\sigma)$ photometric error σ_V. Likewise, the fourth and fifth columns give the $B-V$ color and its rms $(1\,\sigma)$ photometric error $\sigma_{(B-V)}$. We only present photometry of stars with signal-to-noise ratios SNR ≥ 10 in both the F450W and F555W filters. •TAB4 •TAB5 •TAB6 •TAB7 •TAB8

3. COLOR-MAGNITUDE DIAGRAMS

The V versus $B-V$ color-magnitude diagrams of our observed stellar fields in NGC 416, NGC 121, NGC 339, NGC 361, and Kron 3 are displayed in Figs. 2, 3, 4, 5, and 6, respectively. We have arbitrarily split each cluster observation into two regions: (1) the "cluster" region defined as the PC1 CCD, and (2) the SMC "field" region defined as the WF CCDs. Ideally, we should have used a background field that was well outside the tidal radius of the cluster, however we have only one WFPC2 field for each cluster. •FIG2 •FIG3 •FIG4 •FIG5 •FIG6

We used the following procedure to statistically remove the SMC field population from the cluster region CMDs. For a given star in the cluster region CMD of NGC 416 (Fig. 2b) we can count how many stars can be found in that CMD that have $B-V$ colors within MAX$(2\sigma_{(B-V)}, 0.100)$ mag and V magnitudes within MAX$(2\sigma_V, 0.200)$ mag. Let us call that number $N_{\rm NGC416}$. We can also count how many stars can be found in the *field* region CMD of NGC 416 (Fig. 2c) within the same V magnitude range and $B-V$ color range that was determined for the star in the *cluster* region CMD. Let us call that number $N_{\rm SMC}$. The probability, p, that the star in the cluster region CMD is actually a cluster member of NGC 416 can be approximated as

$$p \approx 1 - {\rm MIN}\left(\frac{\alpha N_{\rm SMC}^{\rm UL84}}{N_{\rm NGC416}^{\rm LL95}}, 1.0\right) , \qquad (1)$$

where

$$N_{\rm SMC}^{\rm UL84} \approx (N_{\rm SMC}+1)\left[1 - \frac{1}{9(N_{\rm SMC}+1)} + \frac{1.000}{3\sqrt{N_{\rm SMC}+1}}\right]^3 \qquad (2)$$

(Eq. 9 of Gehrels 1986) is the estimated upper ~84% confidence limit[7] of $N_{\rm SMC}$,

$$N_{\rm NGC416}^{\rm LL95} \approx N_{\rm NGC416}\left[1 - \frac{1}{9N_{\rm NGC416}} - \frac{1.645}{3\sqrt{N_{\rm NGC416}}} + 0.031N_{\rm NGC416}^{-2.50}\right]^3 \qquad (3)$$

is the estimated lower 95% confidence limit of $N_{\rm NGC416}$ (Eq. 14 of Gehrels 1986), and $\alpha \equiv 0.0705$ which is the ratio of the area of the cluster region [~0.314 arcmin^2] to the area of the LMC field region [~4.45 arcmin^2]. The probable cluster membership of any given star can be estimated by picking a uniform random number, $0 \leq p' \leq 1$, and if $p' \leq p$ then the star is said to be a probable cluster member.

We demonstrate this CMD-cleaning method using the first star in Table 4 which has a V magnitude of 19.701±0.011 and a $B-V$ color of 0.796±0.017 mag. We found $N_{\rm NGC416} = 170$ stars on the PC1 CCD (see Fig. 2b) with V magnitudes between 19.501 and 19.901 and $B-V$ colors between 0.696 and 0.896 mag. Similarly, we found $N_{\rm SMC} = 130$ stars on the WF CCDs (see Fig. 2c) within the same V magnitude range and $B-V$ color range. From Eq. 2 we find that $N_{\rm SMC}^{\rm UL84} \approx 142.43$ stars and from Eq. 3 we find that $N_{\rm NGC416}^{\rm LL95} \approx 149.14$ stars. Equation 1 thus gives the probability that this star belongs to the cluster NGC 416 as $p \approx 0.9327$. Our uniform random number generator gave us the value $p' = 0.1384$. Since $p' \leq p$, we claim that this star is a probable cluster member of NGC 416. Based on its position in the color-magnitude diagram of Fig. 2d, we see that this star is probably a helium core-burning horizontal-branch star.

Following the methodology described above, we determined the probable cluster membership for all 3351 stars in the cluster region CMD field of NGC 416 using a uniform random number generator. A total of 2826 stars were found to be probable cluster members and they are displayed in the cleaned cluster CMD (see Fig. 2d). This CMD-cleaning method is probabilistic and Fig. 2d therefore represents only one out of an infinite number of different possible realizations of the cleaned NGC 416 CMD.

Equation 1 was designed to eliminate the strong contamination of young SMC field stars that are clearly seen in the NGC 416 observation. Unfortunately, the clear presence of cluster stars on the WF CCDs (see Fig. 1) indicates that this cleaning procedure represents an "overcleaning" of the true cluster CMDs. Such overcleaning will be most obvious in regions of the color-magnitude diagram where there is rapid luminosity/color evolution or where stellar densities are intrinsically low. An example of both effects can be found in the cleaned cluster CMD of NGC 339 (Fig. 4d) where a large gap is clearly seen in the red giant branch just below the horizontal branch. In as much as most of the contaminating SMC field main-sequence stars have been removed from the resulting cleaned CMDs, we see that Eq. 1 has achieved its design goal. We caution the reader against placing excessive reliance on the actual cluster membership of any particular star in the cleaned CMDs.

---

[7]Corresponding to Gaussian statistics of +1 standard deviation: $\frac{1}{\sigma\sqrt{2\pi}}\int_{-\infty}^{+1\sigma} e^{\frac{-x^2}{2\sigma^2}}\,dx = 0.8413$.

4. REDDENINGS AND METALLICITIES

4.1. Simultaneous Reddening and Metallicity Method

The work of Sarajedini (1994) introduced a method by which the the reddening and metallicity of a globular cluster can be determined simultaneously using a calibration based on several well-observed Galactic globular clusters with abundances measured on the Zinn & West (1984) metallicity scale. All that is required are values for the magnitude level of the horizontal branch (HB), the color of the red giant branch (RGB) at the level of the HB, and the shape and the position of the RGB. The simultaneous reddening and metallicity (SRM) method has subsequently been developed for use with several standard filter combinations[8], and we would like to apply the V vs $B-V$ version to the photometry presented herein. One might wonder if there is some danger in applying the SRM method to clusters with ages that are much younger than those of the Galactic globular clusters. Sarajedini & Layden (1997) discuss the age sensitivity of the SRM method. They conclude that the method is largely insensitive to age effects for red HB clusters older than $\sim$5 Gyr. As we shall see, this applies to all of the clusters in the present work. We acknowledge however that there *might* be small systematic errors remaining in our abundance measurements.

The first step in applying the SRM method is to measure the V magnitude of the red HB clump ($V_{\rm RHB}$). To do this, we follow the procedure described by Sarajedini, Lee, & Lee (1995; hereafter SLL). Figure 7 shows the CMDs of the cluster RGBs and HBs, where we have included existing CCD photometry for Lindsay 113 (Mould *et al.* 1984, see also PAPERI[9]). The rectangles indicate the stars used in the determination of $V_{\rm RHB}$, which are listed in Table 9. The error in this quantity is computed by combining, in quadrature, the standard error of the mean with the estimated error in the photometric zeropoint, which is $\pm$0.05 mag for the *HST* observations and $\pm$0.02 mag for the ground-based observations. The agreement between the $V_{\rm RHB}$ values for the HST cluster observations and existing ground-based measurements for these same clusters is quite reasonable. For example, converting the Kron 3 $B-R$ data of Rich *et al.* (1984) to $B-V$ yields a $V_{\rm RHB}$ value of 19.44 (DH98) in excellent agreement with $V_{\rm RHB}$=19.45 from our HST data. We can perform the same experiment with the NGC 121 $B-R$ data of Stryker *et al.* (1985); this gives $V_{\rm RHB}$=19.66 (albeit for only 7 stars) which agrees with our value to within the errors. Lastly,

•FIG7

•TAB9

---

[8]Various forms of the SRM method: V vs $V-I$ (Sarajedini 1994), R vs $B-R$ (Sarajedini & Geisler 1996), V vs $B-V$ (Sarajedini & Layden 1997), T_1 vs $C-T_1$ (Geisler & Sarajedini 1998).

[9]The Lindsay 113 BR photometry of Mould *et al.* (1984) was converted by us in PAPERI to the BV system using the color transformation equation of Sarajedini & Geisler (1996): $(B-V)_0 = 0.01135 + 0.6184(B-R)_0 - 0.1071(B-R)_0^2 + 0.1249(B-R)_0^3 - 0.0319(B-R)_0^4$. This transformation equation has an rms error of 0.018 mag and was derived by analyzing bright stars from many globular clusters over a wide range of metallicities spanning a color range $-0.2 \leq (B-R) \leq 2.5$ mag. The addition of the new photometry from von Braun et al. (1998), which includes the stars in 4 globular clusters along with the super-metal-rich open cluster NGC 6791, only slightly increases the rms error to 0.019 mag.

DH98 quote $V_{\rm RHB}$=19.36 for NGC 339 based on some unpublished photometry; this is close to our value of 19.46 for this cluster.

The next step is the determination of RGB fiducials for each cluster. This is accomplished via an iterative 2σ rejection polynomial fitting procedure applied to the RGB stars. The resultant fits are plotted in Fig. 7. The analogous diagram for Lindsay 1 is given in Fig. 1 of SLL. From these fits, we measure the value of $(B-V)_g$ which is the $B-V$ color of the RGB at the level of the HB. All of the inputs into the SRM method are now in hand and it is a simple matter to apply the V vs $B-V$ version to our 7 SMC clusters. We also have estimated errors for $V_{\rm RHB}$ and $(B-V)_g$. These are input into the SRM method via a Monte Carlo simulation which yields errors in [Fe/H] and E$(B-V)$ (see Sarajedini 1994 for details).

4.2. Red Giant Branch Slope

Another method we can exploit for the determination of metallicity is the RGB slope. It is well known that the RGB slope steepens with decreasing metallicity. To establish a modern calibration of how metallicity varies with RGB slope, we turn to the photometric data presented by Sarajedini & Layden (1997). In particular, we measure the slopes of the RGBs for all clusters listed in their Table 5. We follow Hartwick (1968) and define the RGB slopes ($S_{-2.0}$ and $S_{-2.5}$) as follows: $S_{-2.0} \equiv -2.0/\left[(B-V)_g - (B-V)_{-2.0}\right]$ and $S_{-2.5} \equiv -2.5/\left[(B-V)_g - (B-V)_{-2.5}\right]$ where we measure the color of the RGB at 2.0 and 2.5 magnitudes above the HB. Table 10 lists •TAB10 the calibration data measured from the RGBs of Sarajedini & Layden (1997) along with the cluster metallicities which are on the Zinn & West (1984) scale. The clusters listed first are their "primary" calibrators and those listed second are their "secondary" calibrators. The two panels of Fig. 8 show our weighted least squares fits to the data. The $S_{-2.0}$ fit has an rms error of 0.19 dex •FIG8 while the $S_{-2.5}$ fit exhibits an rms error of 0.14 dex. We note that, although Lindsay 1 is listed in Table 7, it was not used in the fit because we seek to determine its metallicity via the derived relation.

Once we have established the relations between metallicity and RGB slope, it is a simple matter to measure the slopes for our 7 SMC clusters from the RGB fits. For the two clusters with RGBs that reliably extend 2.5 magnitudes above the HB (NGC 121 and NGC 416), we use the $S_{-2.5}$ calibration; for the others, we apply the $S_{-2.0}$ relation. In all cases, the derived metallicities from the RGB slope are within 0.05 dex of the SRM method determination, lending credence to our techniques. The RGB slope metallicity can then be combined with Equation 1 of Sarajedini & Layden (1997) and the measured value of $(B-V)_g$ to compute the reddening. Again, these reddenings are within 0.01 mag of those yielded by the SRM method.

To arrive at our final adopted values, we perform a weighted mean of the SRM method and the RGB slope results. This process gives us the metallicities and reddenings tabulated in Table 9. A careful inspection of Table 9 shows that the reddening of Kron 3 is a negative value. This is,

of course, not possible, but given the error in the reddening of ±0.02 mag, it is, within the errors, consistent with $E(B-V) = 0$.

Recently, Da Costa & Hatzidimitriou (DH98) have published Ca II triplet metallicities for 5 of the clusters in our sample (Lindsay 1, Kron 3, NGC 121, NGC 339, and Lindsay 113). If we compare our abundances for these clusters with their values, we find a mean difference of $[Fe/H]_{CaII} - [Fe/H] = 0.11 \pm 0.06$ (s.e.m.) when comparing to their metallicities which have not been corrected for age effects (column 2 of Table 3 in Da Costa & Hatzidimitriou) and 0.06 ± 0.08 (s.e.m.) for their age-corrected metallicities (column 3 of Table 3). Note that DH98 utilized the Lindsay 1 photometry of Olszewski *et al.* (1987) in their spectroscopic analysis. In their paper, Olszewski *et al.* (1987) construct a CMD of Lindsay 1 and estimate the V magnitude of the red HB clump to be 19.2 ± 0.1, which DH98 adopt in their work. However, an examination of the Lindsay 1 CMD reveals that this is *clearly* too bright by ∼0.15 mag. Our value for the V_{RHB} of Lindsay 1, which has been determined from the Olszewski *et al.* (1987) data (see SLL), is more faithful to the actual location of this feature. If we correct the DH98 Zinn & West metallicity of Lindsay 1 using the V_{RHB} value in Table 9, we find a decrease of 0.05 dex bringing it closer to our metallicity value. Furthermore, if we adopt a more appropriate age for Kron 3 (see next section), the DH98 age-corrected abundance becomes more metal-poor by ∼0.03 dex, again closer to our value. Taken together, the good agreement between the spectroscopic metallicities and our photometric ones provides a useful check on both methods. Furthermore, it indicates that any systematic errors still present in our metallicities are likely to be small.

5. AGES

The most robust age determination techniques are those that deal with the measurement of relative ages. As such, we have chosen to study the ages of the SMC populous clusters relative to that of Lindsay 1. One would ideally like to utilize the position of the main sequence turnoff (MSTO) to estimate the relative age. However, in the present case, the scatter of the main sequence photometry prohibits us from measuring the precise location of the MSTO. As a result, we must resort to a less direct technique to determine the cluster age. In particular, since our photometry reveals the location of the red HB clump very well, we can utilize the age-determination method described by SLL. They exploit the fact that the color of the red HB clump is dependent on metallicity and age in order to derive the ages of several Galactic globular clusters. After measuring the difference in $B-V$ color between the HB and RGB [$d_{(B-V)}$] and adopting values for the cluster metallicity, SLL use their Fig. 4 to compute the cluster ages. Their Fig. 5 then yields the absolute magnitude of the red HB given the age and metallicity. Both of these calibrations are based on theoretical synthetic HB models. Sarajedini *et al.* (1995) then test their $d_{(B-V)}$ relative ages by comparing them to those yielded by MSTO comparisons. They find that for clusters with [Fe/H] < -0.7 dex, the $d_{(B-V)}$ ages and the MSTO ages agree to within 1 Gyr. We also point out that, since $d_{(B-V)}$ is a purely differential quantity, it is relatively easy to

measure precisely, and it is free from the uncertainties inherent in the photometric zeropoint; it is also reddening and distance independent.

To apply the $d_{(B-V)}$ method of SLL, we must measure the color of the red HB clump and the RGB at the level of the HB. The latter has already been described in previous section. The color of the red HB is simply computed using the stars in the rectangles illustrated in Fig. 7. The associated errors represent the standard error of the mean. This procedure gives us the $d_{(B-V)}$ values listed in Table 9. Figure 4 of SLL then yields the ages tabulated in column 6 of Table 9. The absolute V magnitude of the RHB, $M_V^{\rm RHB}$, is then derived from Fig. 5 of SLL and listed in column 7 of Table 9. We would like to tie our ages to the scale of Olszewski *et al.* (1996) in which Lindsay 1 is 9 ± 1 Gyr old. As a result, we have added 1.3 ± 1.1 Gyr to the $d_{(B-V)}$ ages derived above. Our adopted ages are those surrounded by brackets in Table 9. These ages supersede those published in PAPERI.

We note that, since the youngest age in the calibration of SLL is 7 Gyr, we have had to extrapolate their model grid in order to estimate the ages of Lindsay 113, Kron 3, NGC 339, and NGC 416. We realize that this is not ideal; however, we have no choice given the large errors associated with the main sequence photometry. For the sake of completeness, we note that the extrapolations have been performed using cubic polynomials fitted to the 9 age points (7 to 15 Gyr in units of 1 Gyr) in Fig. 4 of SLL. The root-mean-square (rms) deviations of the fitted points from the fits were never greater than 0.1 Gyr with typical values being ~0.06 Gyr. Because these rms deviations are so small, they were not included in the derived age error.

One way we can verify the resulting ages is to compare the CMDs with theoretical isochrones. This is not the preferred manner in which to measure these ages because of lingering uncertainties in the models, but it does provide a quantitative check on our results. Figures 9 and 10 show the comparisons of the cluster photometry with the theoretical isochrones of Bertelli *et al.* (1994) for the indicated ages and metallicities. Figure 9 displays the three clusters whose metallicities are close to those for which Bertelli *et al.* (1994) tabulate isochrones thus requiring essentially no interpolation within their (coarse) metallicity grid. Figure 10 includes the remaining clusters which require comparisons to isochrones with metallicities that bracket the measured cluster value. The isochrones have been adjusted in the horizontal direction using the reddenings in Table 9 and in the vertical direction by requiring a match between the observed $V_{\rm RHB}$ values and the theoretical location of the red HB. It is evident from Figs. 9 and 10 that the rescaled $d_{(B-V)}$ ages of these clusters (see bracketed values of column 6 of Table 9) are fully consistent with the isochrone fits. This consistency is one piece of evidence that our relative $d_{(B-V)}$ age estimates are robust, even though they are extrapolations.

•FIG9
•FIG10

Another method at our disposal to verify the $d_{(B-V)}$ ages involves direct comparisons between the photometry for each cluster and the fiducial sequence of a comparison cluster. We seek to examine the relative locations of the MSTOs in the same spirit as SLL. Figure 11 illustrates our MSTO comparisons. The strategy is to use the $M_V^{\rm RHB}$ and $E(B-V)$ values in Table 9 to place

•FIG11

the cluster photometry into the Hertzprung-Russell diagram; then we would like to compare each cluster to the fiducial sequence of a standard cluster of similar metallicity. The choice of the standard cluster is obvious given the fact that we have selected Lindsay 1 to set our age scale. However, the metallicity of NGC 121 is too different from that of Lindsay 1 for the latter to serve as an effective standard. As a result, we will utilize the fiducial sequence of Palomar 14 ([Fe/H] $= -1.60$) from Sarajedini (1997) to compare to NGC 121. The clusters are presented in Fig. 11 in order of increasing age from top to bottom and left to right. The primary result of Fig. 11 is that the age ranking derived from the $d_{(B-V)}$ method is corroborated by the relative locations of the MSTOs. Notice, for example, the locations of the subgiant branches (i.e. the nearly horizontal sequence that links the MSTO and RGB); the magnitude of the SGBs approaches that of the standard cluster fiducials as age increases. Another feature to notice about Fig. 11 is that the RGBs of all the clusters line up quite well with that of the standard cluster, thus supporting our metallicity measurements. In addition, we note that the color of the red HB clump becomes progressively bluer for older clusters, as it should, an effect also pointed out in the review article by Sarajedini et al. (1997).

There are existing age determinations for some of the SMC clusters presented herein. For example, Mould *et al.* (1984) utilize their $B-R$ CCD photometry to estimate an age of 5 Gyr for Lindsay 113 when placed at a distance modulus of $(m-M)_0 = 18.80$ and $[M/H] = -1.4$ is adopted. Using similar parameters, Olszewski *et al.* (1987) find an age of 10 Gyr for Lindsay 1, while Stryker *et al.* (1985) conclude that NGC 121 is 12 Gyr old. All three of these ages are in excellent agreement with those estimated in this study. In the case of Lindsay 113, this is not unexpected since the photometry we use to derive an age is simply that of Mould *et al.* (1984) converted from $B-R$ to $B-V$ (see Sec. 4.1). For Kron 3, the work of Rich *et al.* (1984) yields an age between 5 and 8 Gyr; in contrast, Alcaino *et al.* (1996) conclude that the age of Kron 3 is 10 Gyr with a lower limit of 8 Gyr. The recent work of DH98 concerning the Ca II triplet metallicities of these clusters has adopted 9 Gyr for the age of Kron 3. Based on the relative location of the red HB clump as well as the MSTO, we have shown in this paper that the age of Kron 3 is closer to 6 Gyr, thus corroborating the original age estimate of Rich *et al.* (1984). When we compare the Kron 3 CMD of Alcaino *et al.* (1996) with our photometry, we find generally good agreement in terms of the magnitude of the MSTO. As a result, it is unclear to us at this point why Alcaino *et al.* (1996) derive a much older age for Kron 3.

6. DISCUSSION

The exhaustive reduction and analysis presented so far will now provide the foundation for the remainder of the paper in which we hope to shed light on the star formation history (SFH) of the SMC. To facilitate this, Fig. 12 shows the relationship between age and metallicity for the SMC clusters (filled circles) considered herein. The open circles are the younger SMC clusters taken from the discussion presented by DH98 (see DH98 for references). The remaining three points, the asterisk, diamond, and square, are the present-day abundance of the SMC taken from Luck & Lambert (1992), Russell & Bessell (1989), and Hill (1997), respectively. The points marked as × are LMC clusters; the data for clusters older than 10 Gyr are from Olsen *et al.* (1998) and the younger cluster data are from Geisler *et al.* (1997) and Bica *et al.* (1998). From the appearance of this figure, we note the following points. First, assuming that cluster destruction processes and cluster fading with age are similar in the LMC and SMC, it is clear that, in general, these two galaxies have had very different SFHs. In particular, at a given age, the mean abundance of the SMC clusters is ∼0.3 dex lower than that of the LMC clusters (Olszewski et al. 1996); this is a restatement of the observation that for dwarf galaxies, the mean metal abundance is correlated with the total absolute luminosity in the sense that more metal-rich systems are brighter (Sarajedini *et al.* 1997, and references therein). However, Fig. 12 allows us to draw more specific conclusions than this. For example, when considering only the clusters with ages less than ∼10 Gyr, it seems that between ∼3 and ∼10 Gyr ago, the LMC experienced a rapid chemical enrichment (Geha *et al.* 1998) that the SMC did not, or perhaps the chemical enrichment of the LMC was simply more vigorous than that of the SMC (Pagel & Tautvaišienė 1998). •FIG12

The star formation history derived from the LMC clusters differs markedly from that indicated by the field stars (Geha *et al.* 1998; Olszewski *et al.* 1996; Sarajedini 1998). There is tenuous evidence that, in the case of the SMC, the SFHs of the clusters and field stars maybe quite similar (e.g. DH98; Gardiner & Hatzidimitriou 1992). Sarajedini (1998) argues that this apparent difference between the LMC and the SMC is due to the fact that there are probably more clusters in the LMC age gap (between 2.5 and 9 Gyr) than are currently known. Much work has been done on the young field stars in the Magellanic Clouds, however progress towards understanding the early SFH of the Clouds can only be achieved by analyzing the old (i.e. faint) field stellar population. While the analysis of a few *HST* WFPC2 fields (e.g. Gallagher *et al.* 1996; Holtzman *et al.* 1997; Geha *et al.* 1998) has shown the clear potential of such research for understanding of the early SFH of the LMC, comparable studies in the SMC do not yet exist.

Figure 13 compares our age-metallicity data for the SMC with two theoretical representations of its SFH. Under the assumption of chemical homogeneity, the top panel shows the result of treating the SMC as a simple closed-box system with continuous star formation, kindly provided by Gary Da Costa and illustrated in Fig. 4 of DH98, whereas the lower panel depicts the bursting SFH of Pagel & Tautvaišienė (1998). The SMC is almost certainly not a closed-box, but comparisons such as these allow us to distinguish between a continuous and bursting SFH. Indeed, the upper panel showing the continuous star formation is an exceedingly poor fit to the age-abundance data. •FIG13

Of the older clusters considered here, only the error bars associated with NGC 121 and perhaps Lindsay 1 are consistent with this curve. In contrast, the theoretical relation shown in the bottom panel is a better fit to the observational data. The majority of the clusters intersect the solid curve to within their 1σ error bars. The three possible exceptions are NGC 416, NGC 361, and NGC 339. The bursting star formation model formulated by Pagel & Tautvaišienė (1998) can be adjusted to fit the age-metallicity data for the SMC. For example, the existing form of their model postulates an initial star formation burst that began 14 Gyr ago and peaked ~11.3 Gyr ago. Then the star formation rate (SFR) decreased and remained constant until 4 Gyr ago (see their Fig. 2). If we adjust their model so that the initial burst of star formation lasted for only 2 Gyr as opposed to 2.7 Gyr, then it is possible that the age-metallicity relation would provide a better fit to all of the older clusters. With this one revision, the SFH outlined by Pagel & Tautvaišienė (1998) would be an excellent fit to the age-abundance data for the clusters in the SMC.

7. CONCLUSIONS AND FUTURE WORK

We have presented new *HST* WFPC2 photometry for 5 star clusters in the Small Magellanic Cloud. Along with the published data for two other clusters, we derive more precise values for the cluster metallicities and ages as compared with previous studies. Knowledge of these quantities has allowed us to improve our understanding of the age-metallicity relation of the SMC clusters, and provided, for the first time, a consistent picture for the star formation and chemical enrichment history of the SMC.

Figure 14 compares the probable cluster members with the nearby SMC field stellar population. While the cluster/field separation scheme used in this paper could be improved, one can nevertheless draw several conclusions from this figure which might be helpful to researchers designing future studies of the populous star clusters in the Small Magellanic Cloud. First, the youngest stars in the SMC field stellar population near the populous clusters cover a large age range of over 10 Gyr. The bright blue main-sequence stars of Fig. 2c indicate that the SMC field stellar population near NGC 416 is young (<1 Gyr) while the age of the SMC field near Kron 3 and NGC 121 is 7±2.5 and 11±2.5 Gyr, respectively (Gardiner & Hatzidimitriou 1992). Second, while the red giant branches of the field and cluster populations are nearly identical, one sees many field subgiant branch (SGB) stars which are significantly brighter than the average cluster subgiant branch star at the same $B-V$ color. This is consistent with the interpretation that the SMC field stellar population near the populous clusters have intermediate-age metal-poor components which are slightly younger than the nearby cluster but of similar metallicity (assuming the distance to the cluster and field are the same). Third, the spread of $B-V$ color near the base of the red giant branch is anomalously large for some of the cluster CMDs (e.g. NGC 121). This is most likely a result of inadequate CMD cleaning due to poor sampling of the SMC field subgiant branch stellar population. Better sampling of the SMC field SGB stars is required for the identification of probable field SGB stars. Since SGB stars are expected to be relatively rare

•FIG14

in any given observation of the SMC field, due to their rapid luminosity and color evolution, one must then observe a lot of the nearby SMC field in order to adequately determine the luminosity and color properties of the field SGB population. In other words, the accurate determination of the age of an SMC populous cluster via the analysis of main-sequence-turnoff photometry requires the proper identification of probable SMC field SGB stars — one WFPC2 field-of-view is clearly inadequate for some clusters. Deeper observations with better field coverage are thus required in order to obtain unambiguous astrophysical interpretations of the cluster/field star formation histories of the Small Magellanic Cloud.

We thank Gary Da Costa for the timely provision of his SMC star formation history models. We would like to thank the anonymous referee whose comments and suggestions have improved the final product presented here. KJM was supported by a grant from the National Aeronautics and Space Administration (NASA), Order No. S-67046-F, which was awarded by the Long-Term Space Astrophysics Program (NRA 95-OSS-16). AS was supported by the NASA grant number HF-01077.01-94A from the Space Telescope Science Institute, which is operated by the Association of Universities for Research in Astronomy, Inc., under NASA contract NAS5-26555. AS wishes to thank Lick Observatory for their generosity and hospitality during his visit. Figure 1 was created with images from the Digitized Sky Survey[10]. This research has made use of NASA's Astrophysics Data System Abstract Service and the NASA/IPAC Extragalactic Database (NED) which is operated by the Jet Propulsion Laboratory at the California Institute of Technology, under contract with NASA.

---

[10]Based on photographic data obtained using The UK Schmidt Telescope. The UK Schmidt Telescope was operated by the Royal Observatory Edinburgh, with funding from the UK Science and Engineering Research Council, until 1988 June, and thereafter by the Anglo-Australian Observatory. Original plate material is copyright (c) the Royal Observatory Edinburgh and the Anglo-Australian Observatory. The plates were processed into the present compressed digital form with their permission. The Digitized Sky Survey was produced at the Space Telescope Science Institute under US Government grant NAG W-2166.

REFERENCES

Alciano, G., Liller, W., Alvarado, F., Kravtsov, V., Ipatov, A., Samus, N., & Smirnov, O. 1996, AJ, 112, 2004

Arp, H.C. 1958, AJ, 63, 487

Bertelli, G., Bressan, A., Chiosi, C., Fagotto, F., & Nasi, E. 1994, A&AS, 106, 275

Bica, E., Geisler, D., Dottori, H, Clariá, J.J., Piatti, A.E., & Santos, Jr., J.F.C. 1998, AJ (in press) [preprint: `http://xxx.lanl.gov/abs/astro-ph/9803167`]

Biretta, J. A. *et al.* 1996, WFPC2 Instrument Handbook, Version 4.0 (STScI, Baltimore)

Brocato, E., Castellani, V., Ferraro, F.R., Piersimoni, A.M., & Testa, V. 1996, MNRAS, 282, 614

Da Costa, G. S. 1991, in The Magellanic Clouds, IAU Symp. 148, ed. R. Haynes & D. Milne (Kluwer: Dordrecht), p. 183

Da Costa, G. S., & Hatzidimitriou, D. 1998, AJ, 115, 1934 (DH98)

Gardiner, L.T., & Hatzidimitriou, D. 1992, MNRAS, 257, 195

Gallagher, J.S. *et al.* 1996, ApJ, 466, 732

Gascoigne, S.C.B. 1966, MNRAS, 134, 59

Geha, M.C., *et al.* 1998, AJ, 115, 1045

Gehrels, N. 1986, ApJ, 303, 336

Geisler, D., & Sarajedini, A. 1998, AJ (submitted)

Geisler, D., Bica, E., Dottori, H., Clariá, J.J., Piatti, A.E., Santos, Jr., J.F.C., 1997, AJ, 114, 1920

Hartwick, F.D.A. 1968, ApJ, 154, 475

Hill, V. 1997, A&A, 324, 435

Holtzman, J. A., *et al.* 1995a, PASP, 107, 1065

Holtzman, J.A., *et al.* 1995b, PASP, 107, 156

Holtzman, J.A., *et al.* 1997, AJ, 113, 656

Luck, R. E., & Lambert, D. L. 1992, ApJS, 79, 303

Mighell, K. J. 1997, AJ, 114, 1458

Mighell, K.J., Rich, R.M., Shara, M., & Fall, S.M. 1996, AJ, 111, 2314

Mighell, K.J., Sarajedini, A., & French, R.S. 1998, ApJ, 494, L189 (PAPERI)

Mould, J.R., Da Costa, G.S., & Crawford, M.D. 1984, ApJ, 280, 595

Olsen, K.A.G., Hodge, P.W., Mateo, M., Olszewski, E.W., Schommer, R.A., Suntzeff, N.B. Walker, A.R. 1998, MNRAS (in press) [preprint: `http://xxx.lanl.gov/abs/astro-ph/9806023`]

Olszewski, E.W., Schommer, R.A., & Aaronson, M. 1987, AJ, 93, 565

Olszewski, E.W., Suntzeff, N.B., & Mateo, M. 1996, ARA&A, 34, 511

Russell, S. C. & Bessell, M. S. 1989, ApJS, 70, 865

Pagel, B.E.J., & Tautvaišienė, G. 1998, MNRAS (submitted) [preprint: `http://xxx.lanl.gov/abs/astro-ph/9801221`]

Rich, R. M., Da Costa, G. S., & Mould, J. R. 1984, ApJ, 286, 517

Sarajedini, A. 1994, AJ, 107, 618

Sarajedini, A. 1997, AJ, 113, 682

Sarajedini, A. 1998 (submitted)

Sarajedini, A., Chaboyer, B., & Demarque, P. 1997, PASP, 109, 1321

Sarajedini, A., & Geisler, D. 1996, AJ, 112, 2013

Sarajedini, A., Geisler, D., Schommer, R., & Harding, P. 1997, BAAS, 190, #35.03

Sarajedini, A., & Layden, A.C. 1997, AJ, 113, 264

Sarajedini, A., Lee, Y.-W., & Lee, D.-H. 1995, ApJ, 450, 712 (SLL)

Stryker, L. L., Da Costa, G. S., & Mould, J. R. 1985, ApJ, 298, 544

von Braun, K., Chiboucas, K., Minske, J.K., Salgado, J.F., & Worthey, G. 1998, PASP (in press) [preprint: `http://xxx.lanl.gov/abs/astro-ph/9804001`]

Walker, A.R. 1993, AJ, 106, 999

Zinn, R., & West, M.J. 1984, ApJS, 55, 45

This preprint was prepared with the AAS LaTeX macros v4.0.

TABLE 1. Observation log

FIELD	DATASETS	FILTER	EXP (s)	R.A. α (2000.0)	DEC. δ	V3 (°)	OBS-DATE
NGC 121	U26M0101T	F450W	600.000	00 26 42.910	-71 31 57.144	295.649	01/26/94 23:28:17
	U26M0102T	F555W	300.000				23:42:17
NGC 339	U26M0201T	F450W	400.000	00 57 45.000	-74 28 11.600	1.955	04/07/94 18:03:17
	U26M0202T	F555W	200.000				18:13:17
NGC 361	U26M0601T	F450W	300.000	01 02 10.100	-71 36 21.099	356.762	04/03/94 08:38:17
	U26M0602T	F555W	160.000				08:47:17
NGC 416	U26M0501T	F450W	400.000	01 07 59.100	-72 21 25.999	297.855	02/06/94 21:24:17
	U26M0502T	F555W	200.000				21:34:17
Kron 3	U26M0G01T[a]	F450W	600.000	00 24 46.300	-72 47 38.400	53.894	05/27/94 16:55:17
	U26M0G02T[a]	F555W	300.000				17:09:17

[a]Target name incorrectly designated as ES0121.

TABLE 2. Average aperture corrections $\langle \Delta_r \rangle$ for $r = 2.0$ pixels

Filter	CCD	$\langle \Delta_r \rangle$ (mag)
F450W	PC1	−0.331±0.018
	WF2	−0.153±0.008
	WF3	−0.202±0.017
	WF4	−0.167±0.007
F555W	PC1	−0.376±0.017
	WF2	−0.162±0.010
	WF3	−0.214±0.017
	WF4	−0.178±0.008

TABLE 3. Zero-order ("breathing") aperture corrections δ_r for $r = 2.0$ pixels.

FIELD	FILTER	DATASETS	EXPTIME	δ_r [a]			
			(s)	PC1	WF2	WF3	WF4
NGC 121	F450W	U26M0101T	600.0	+0.009	+0.016	+0.043	+0.025
	F555W	U26M0102T	300.0	+0.018	+0.019	+0.049	+0.026
NGC 339	F450W	U26M0201T	600.0	+0.031	+0.020	+0.044	+0.026
	F555W	U26M0202T	300.0	+0.036	+0.021	+0.052	+0.026
NGC 361	F450W	U26M0601T	300.0	+0.035	+0.006	+0.031	+0.011
	F555W	U26M0602T	160.0	+0.040	+0.013	+0.037	+0.019
NGC 416	F450W	U26M0501T	600.0	+0.026	+0.015	+0.036	+0.015
	F555W	U26M0502T	300.0	+0.026	+0.016	+0.042	+0.016
Kron 3	F450W	U26M0G01T	600.0	+0.033	+0.005	+0.028	+0.011
	F555W	U26M0G02T	300.0	+0.029	+0.002	+0.020	+0.008

[a]The rms error for all values of δ_r is estimated to be 0.005 mag.

TABLE 4. WFPC2 stellar photometry of the SMC cluster NGC 416.*

ID	V (mag)	σ_V (mag)	$B-V$ (mag)	$\sigma_{(B-V)}$ (mag)
106084534	19.701	0.011	0.796	0.017
106211615	21.402	0.023	0.809	0.036
106113662	22.326	0.039	0.502	0.055
106236091	22.357	0.041	0.497	0.060
106207387	23.418	0.075	0.382	0.105

*The entire contents of Table 4 are available at _____. The first 2826 stars are the probable cluster members shown in Fig. 2d. Only the first 5 stars are shown here for form and content.

TABLE 5. WFPC2 stellar photometry of the SMC cluster NGC 121.*

ID	V (mag)	σ_V (mag)	$B-V$ (mag)	$\sigma_{(B-V)}$ (mag)
106076270	22.889	0.049	0.383	0.067
106181472	22.782	0.040	0.394	0.057
106162605	22.637	0.038	0.386	0.053
106203583	19.804	0.009	0.899	0.014
106281909	23.550	0.063	0.576	0.093

*The entire contents of Table 5 are available at _____. The first 3696 stars are the probable cluster members shown in Fig. 3d. Only the first 5 stars are shown here for form and content.

TABLE 6. WFPC2 stellar photometry of the SMC cluster NGC 339.*

ID	V (mag)	σ_V (mag)	$B-V$ (mag)	$\sigma_{(B-V)}$ (mag)
106181871	22.534	0.041	0.593	0.060
106194358	23.218	0.062	0.679	0.092
106207180	22.611	0.040	0.389	0.057
106383794	19.545	0.009	0.728	0.014
106364757	23.874	0.094	0.512	0.129

*The entire contents of Table 6 are available at _____. The first 773 stars are the probable cluster members shown in Fig. 4d. Only the first 5 stars are shown here for form and content.

TABLE 7. WFPC2 stellar photometry of the SMC cluster NGC 361.*

ID	V (mag)	σ_V (mag)	$B-V$ (mag)	$\sigma_{(B-V)}$ (mag)
106281668	24.241	0.112	0.400	0.158
106325961	20.801	0.019	0.710	0.030
106297636	23.566	0.076	0.025	0.101
106472917	23.890	0.086	-0.026	0.113
106575538	22.793	0.052	0.498	0.081

*The entire contents of Table 7 are available at _____. The first 1241 stars are the probable cluster members shown in Fig. 5d. Only the first 5 stars are shown here for form and content.

TABLE 8. WFPC2 stellar photometry of the SMC cluster Kron 3.*

ID	V (mag)	σ_V (mag)	$B-V$ (mag)	$\sigma_{(B-V)}$ (mag)
106071202	22.731	0.037	0.331	0.052
106073871	23.850	0.076	0.638	0.116
106094717	22.979	0.042	0.413	0.061
106174577	23.786	0.070	0.142	0.090
106195751	18.599	0.005	0.965	0.009

*The entire contents of Table 8 are available at _____. The first 2012 stars are the probable cluster members shown in Fig. 5d. Only the first 5 stars are shown here for form and content.

TABLE 9. Cluster parameters.

Cluster	[Fe/H]	E($B-V$) (mag)	$V_{\rm RHB}$ (mag)	$d_{(B-V)}$ (mag)	Age (Gyr)	$M_V^{\rm RHB}$ (mag)
Lindsay 113	−1.24±0.11	0.00±0.02	19.15±0.02	0.117±0.006	4.0±0.7 [5.3±1.3]	0.32±0.04
Kron 3	−1.16±0.09	−0.03±0.02	19.45±0.05	0.125±0.004	4.7±0.6 [6.0±1.3]	0.36±0.03
NGC 339	−1.50±0.14	0.03±0.04	19.46±0.05	0.120±0.007	5.0±0.6 [6.3±1.3]	0.36±0.04
NGC 416	−1.44±0.12	0.08±0.03	19.74±0.05	0.128±0.004	5.6±0.3 [6.9±1.1]	0.40±0.02
NGC 361	−1.45±0.11	0.07±0.03	19.53±0.05	0.141±0.006	6.8±0.5 [8.1±1.2]	0.45±0.02
Lindsay 1	−1.35±0.08	0.06±0.02	19.34±0.02	0.152±0.005	7.7±0.4 [≡ 9.0 ± 1.0]	0.49±0.02
NGC 121	−1.71±0.10	0.05±0.03	19.73±0.05	0.235±0.005	10.6±0.7 [11.9±1.3]	0.55±0.02

NOTE. – Bracketed age estimates assume that Lindsay 1 is 9.0 Gyr old.

TABLE 10. RGB slope data.

Cluster	[Fe/H]	$S_{-2.0}$	$S_{-2.5}$
47 Tuc	−0.71±0.07	4.13	3.11
NGC 1851	−1.29±0.07	5.13	4.17
NGC 6752	−1.54±0.09	5.73	5.07
M68	−2.09±0.11	7.41	6.19
M15	−2.17±0.07	7.41	6.51
NGC 5053	−2.41±0.12	7.19	6.38
NGC 6352	−0.60±0.08	3.11	2.68
ESO121-SC03	−0.93±0.10	4.57	4.12
Lindsay 1	−1.10±0.10	5.41	4.62
NGC 362	−1.27±0.07	5.71	4.45
NGC 1261	−1.31±0.09	6.45	5.04
NGC 288	−1.40±0.12	5.22	4.45
Eridanus	−1.41±0.11	5.04	4.24
Pal 14	−1.60±0.18	6.41	5.22
NGC 1904	−1.69±0.09	6.69	5.42
NGC 6535	−1.75±0.15	6.17	5.62
NGC 6397	−1.91±0.14	7.38	6.44

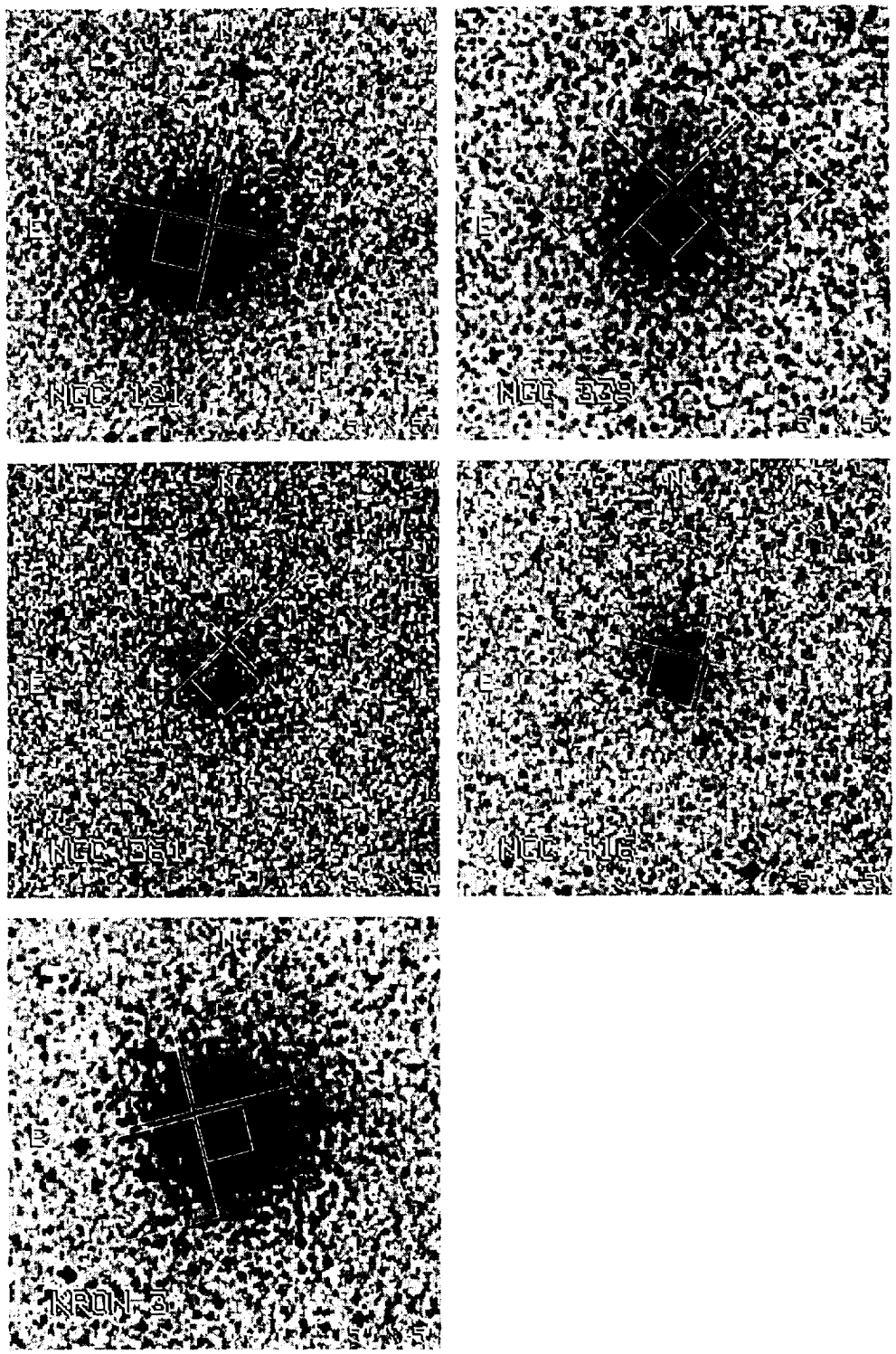

Fig. 1.— Digitized Sky Survey images showing the observed populous clusters in the Small Magellanic Clouds: NGC 121, NGC 339, NGC 361, NGC 416, and Kron 3. The outlines indicate the measured field-of-view of the *Hubble Space Telescope* WFPC2 cameras at the four target positions (see Table 1). Each subfield shown subtends $5'$ on a side. The orientation is North to the top and East to the left.

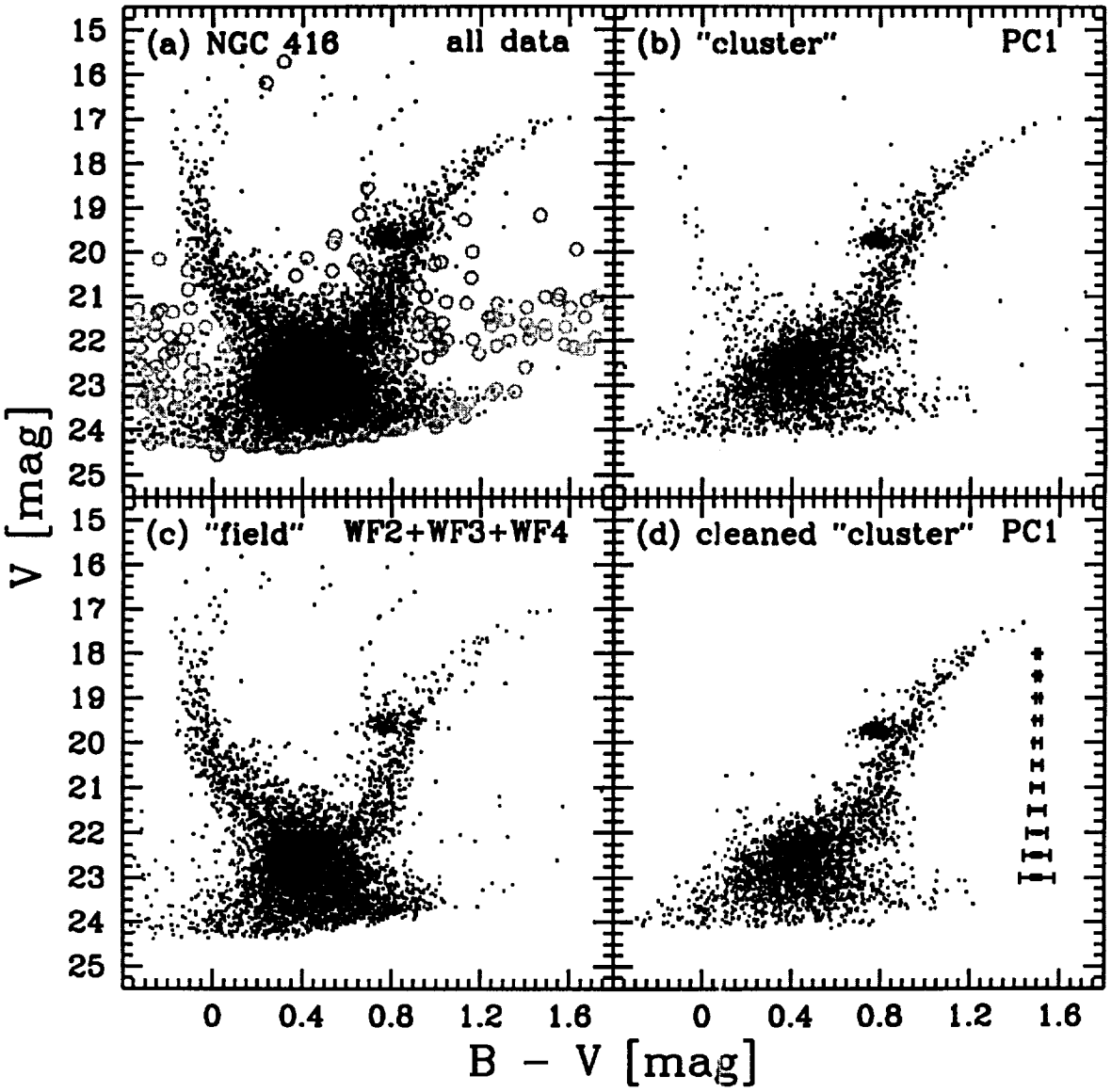

Fig. 2.— The V vs $B-V$ color-magnitude diagram of the observed stellar field in the SMC populous cluster NGC 416. (a) The 8513 stars with signal-to-noise ratios S/N$\geq$10 in both filters are plotted (dots) along with the 2226 CCD/image defects (open circles). (b) The 3351 stars found on the PC1 CCD. (c) The 5162 stars found on the WF2, WF3, and WF4 CCDs. (d) The "cleaned" color-magnitude diagram of NGC 416 contains 2826 stars. The error bars indicate rms (1σ) uncertainties for a single star at the corresponding magnitude.

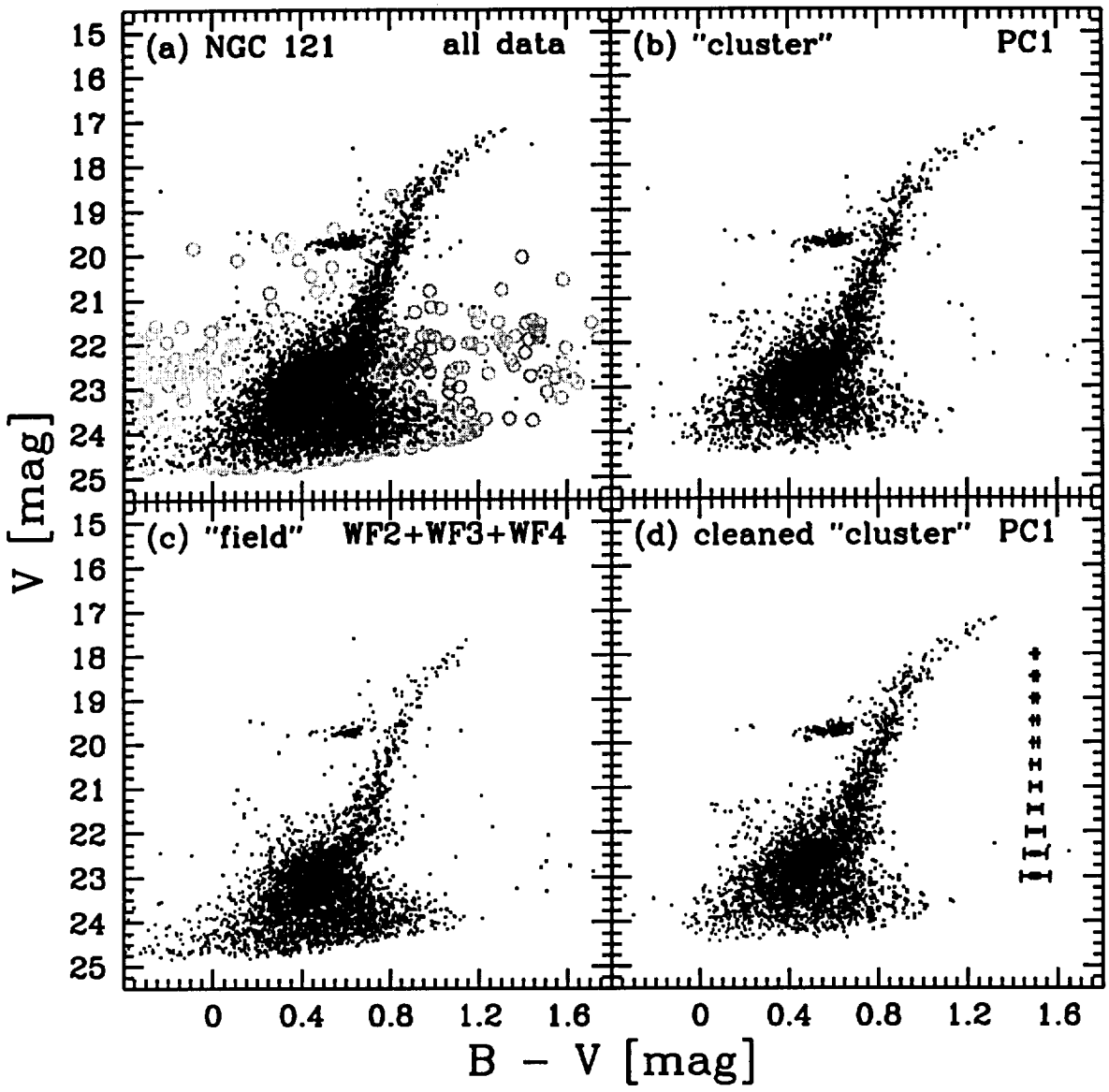

Fig. 3.— The V vs $B-V$ color-magnitude diagram of the observed stellar field in the SMC populous cluster NGC 121. **(a)** The 8133 stars with signal-to-noise ratios S/N$\geq$10 in both filters are plotted (dots) along with the 2128 CCD/image defects (open circles). **(b)** The 4071 stars found on the PC1 CCD. **(c)** The 4062 stars found on the WF2, WF3, and WF4 CCDs. **(d)** The "cleaned" color-magnitude diagram of NGC 121 contains 3696 stars. The error bars indicate rms (1σ) uncertainties for a single star at the corresponding magnitude.

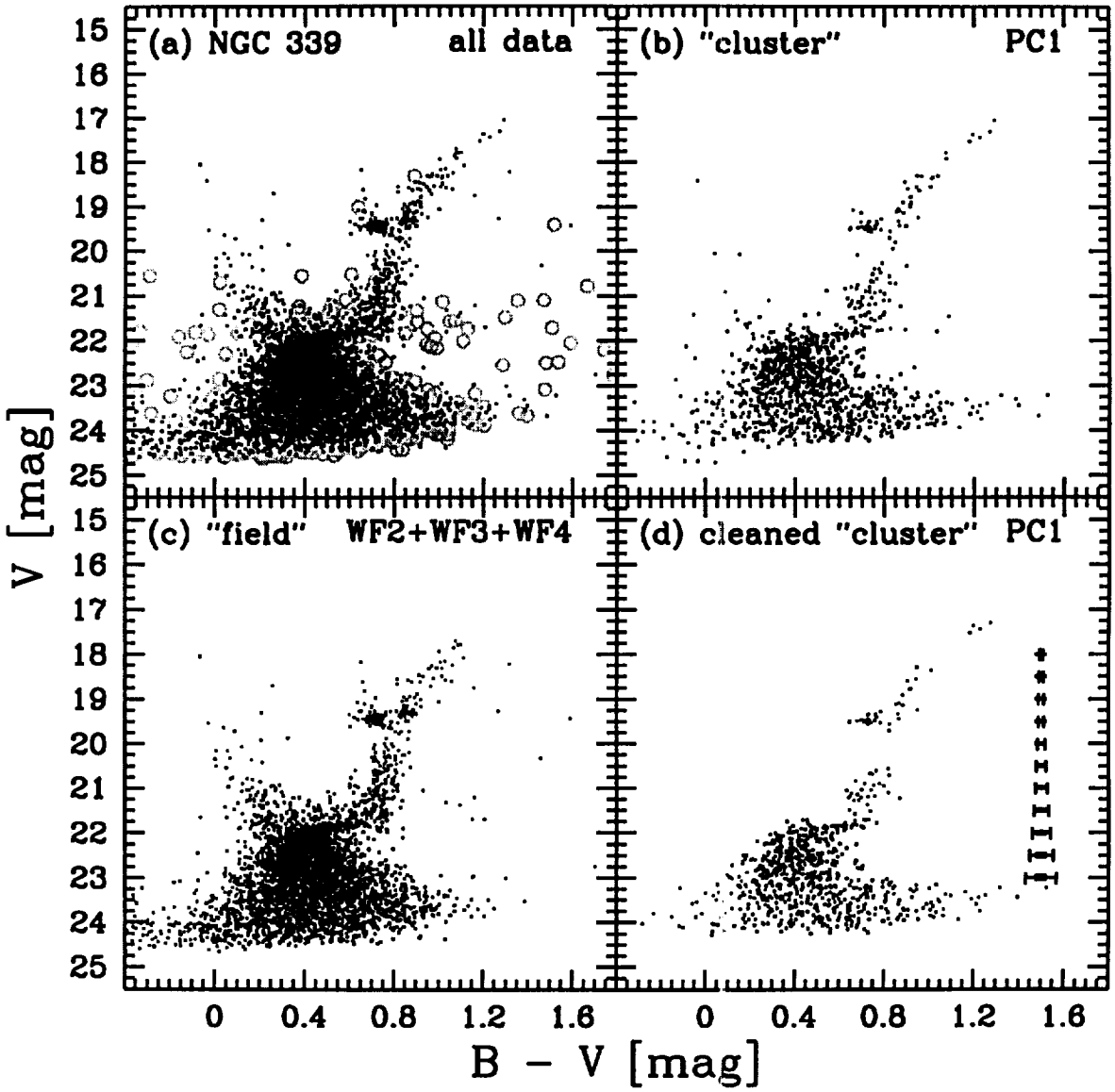

Fig. 4.— The V vs $B-V$ color-magnitude diagram of the observed stellar field in the SMC populous cluster NGC 339. (a) The 5245 stars with signal-to-noise ratios S/N$\geq$10 in both filters are plotted (dots) along with the 1377 CCD/image defects (open circles). (b) The 1199 stars found on the PC1 CCD. (c) The 4046 stars found on the WF2, WF3, and WF4 CCDs. (d) The "cleaned" color-magnitude diagram of NGC 339 contains 773 stars. The error bars indicate rms (1σ) uncertainties for a single star at the corresponding magnitude.

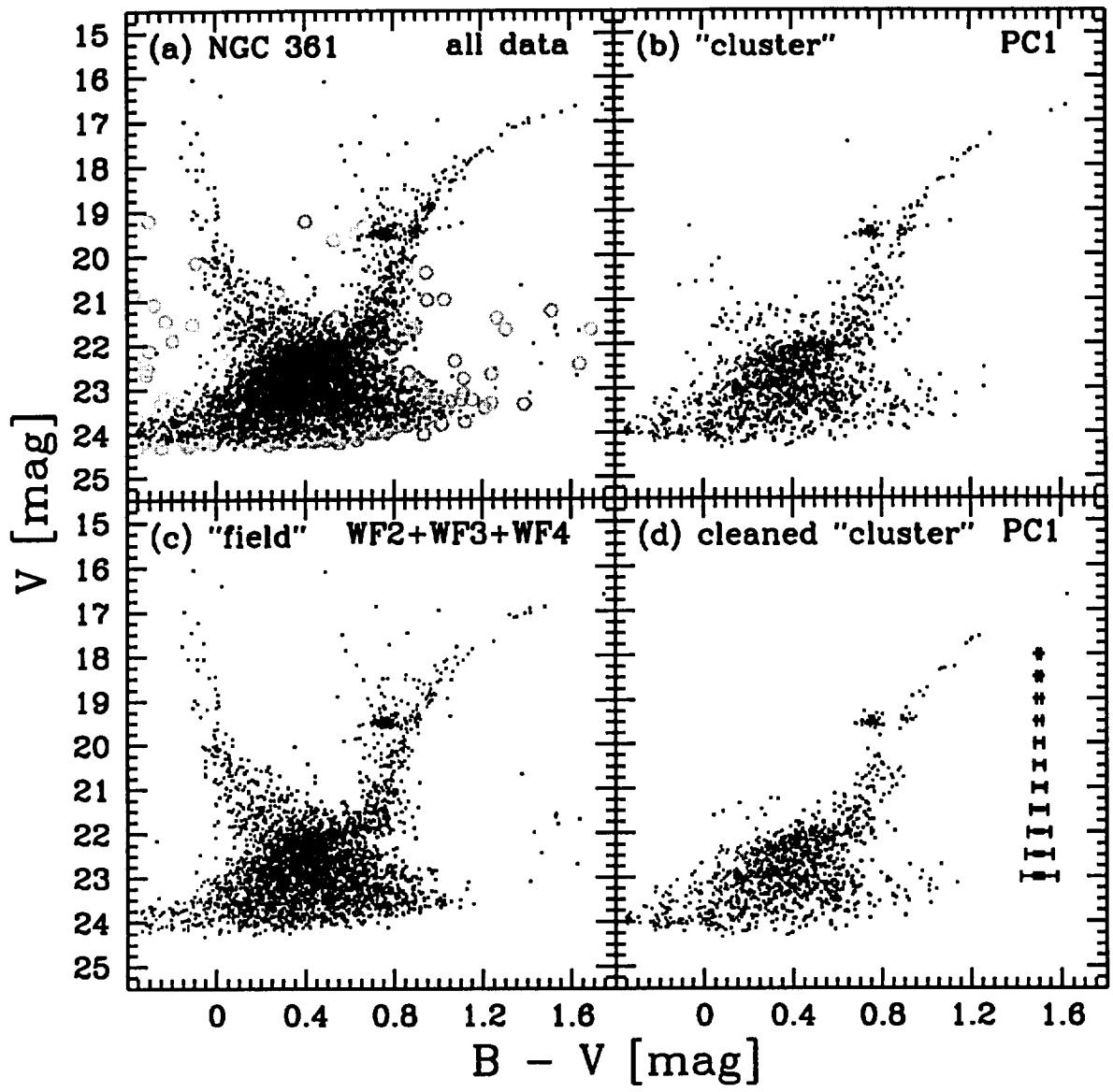

Fig. 5.— The V vs $B-V$ color-magnitude diagram of the observed stellar field in the SMC populous cluster NGC 361. **(a)** The 5172 stars with signal-to-noise ratios S/N$\geq$10 in both filters are plotted (dots) along with the 1420 CCD/image defects (open circles). **(b)** The 1607 stars found on the PC1 CCD. **(c)** The 3565 stars found on the WF2, WF3, and WF4 CCDs. **(d)** The "cleaned" color-magnitude diagram of NGC 361 contains 1241 stars. The error bars indicate rms (1σ) uncertainties for a single star at the corresponding magnitude.

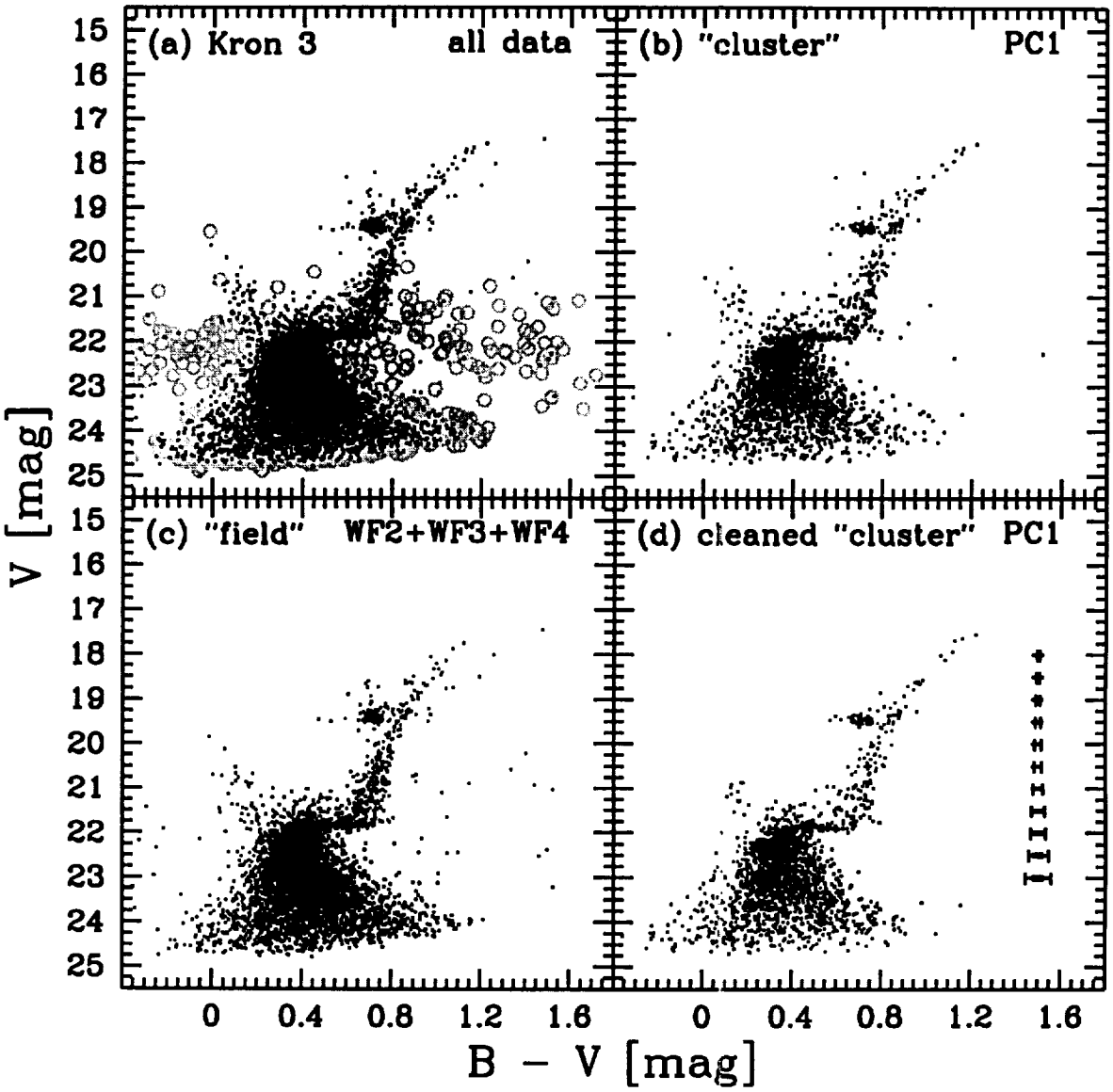

Fig. 6.— The V vs $B-V$ color-magnitude diagram of the observed stellar field in the SMC populous cluster Kron 3. (**a**) The 7669 stars with signal-to-noise ratios S/N$\geq$10 in both filters are plotted (dots) along with the 1990 CCD/image defects (open circles). (**b**) The 2596 stars found on the PC1 CCD. (**c**) The 5073 stars found on the WF2, WF3, and WF4 CCDs. (**d**) The "cleaned" color-magnitude diagram of Kron 3 contains 2102 stars. The error bars indicate rms (1σ) uncertainties for a single star at the corresponding magnitude.

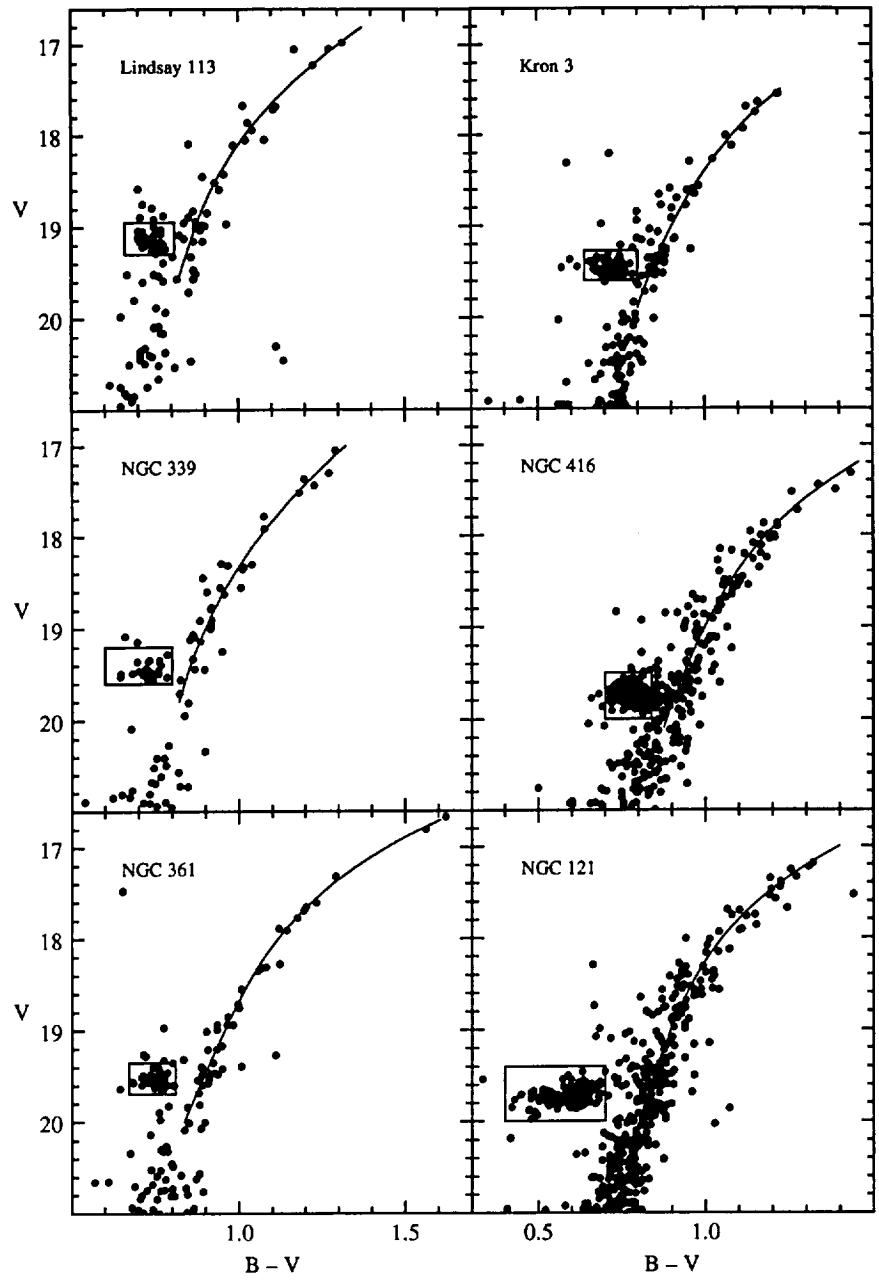

Fig. 7.— Color-magnitude diagrams for 6 of the 7 SMC clusters discussed in this paper showing the horizontal and red giant branches. The rectangles indicate the stars used in the calculation of $V_{\rm RHB}$ while the solid lines in each panel show the polynomial fits resulting from the iterative 2σ rejection technique.

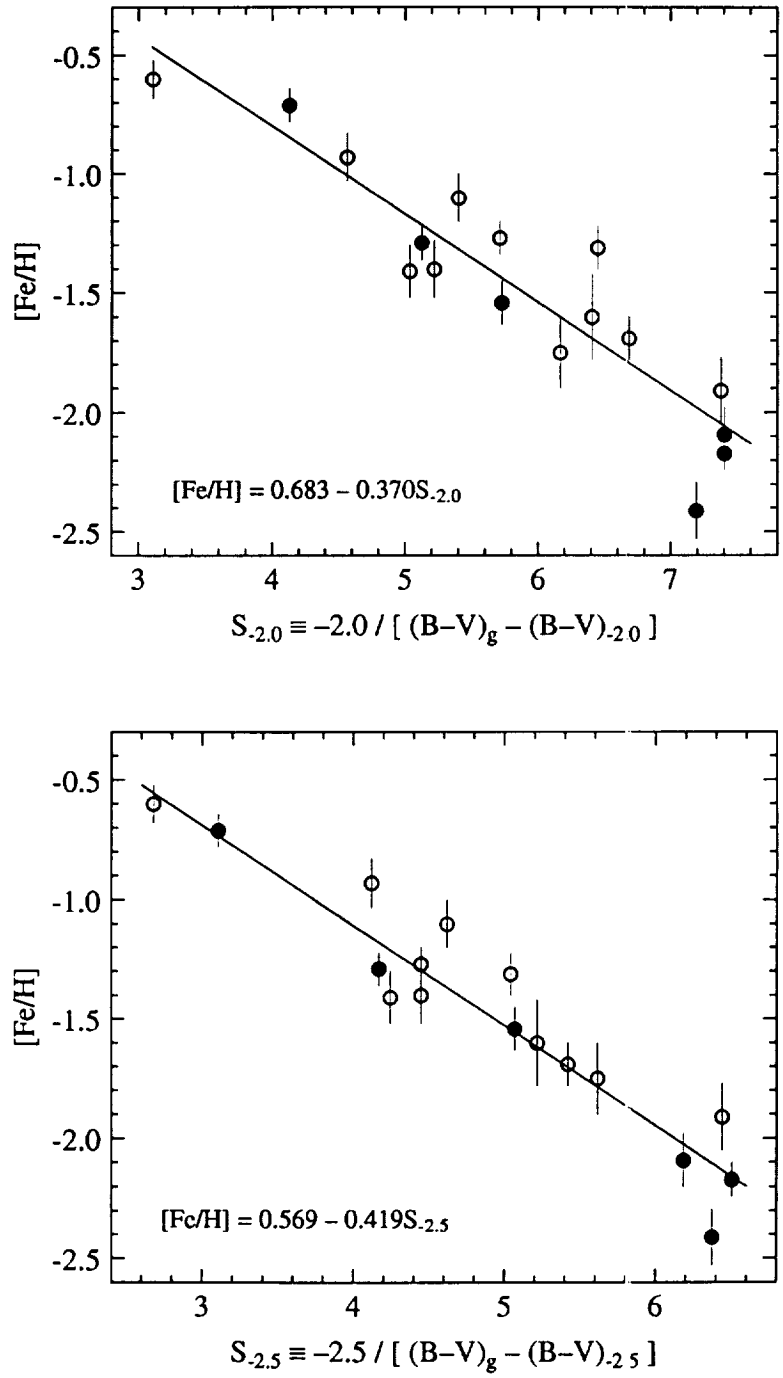

Fig. 8.— Metallicity as a function of the slope of the red giant branch. The primary (**filled circles**) and secondary (**open circles**) calibrators from Sarajedini & Layden (1997) are shown.

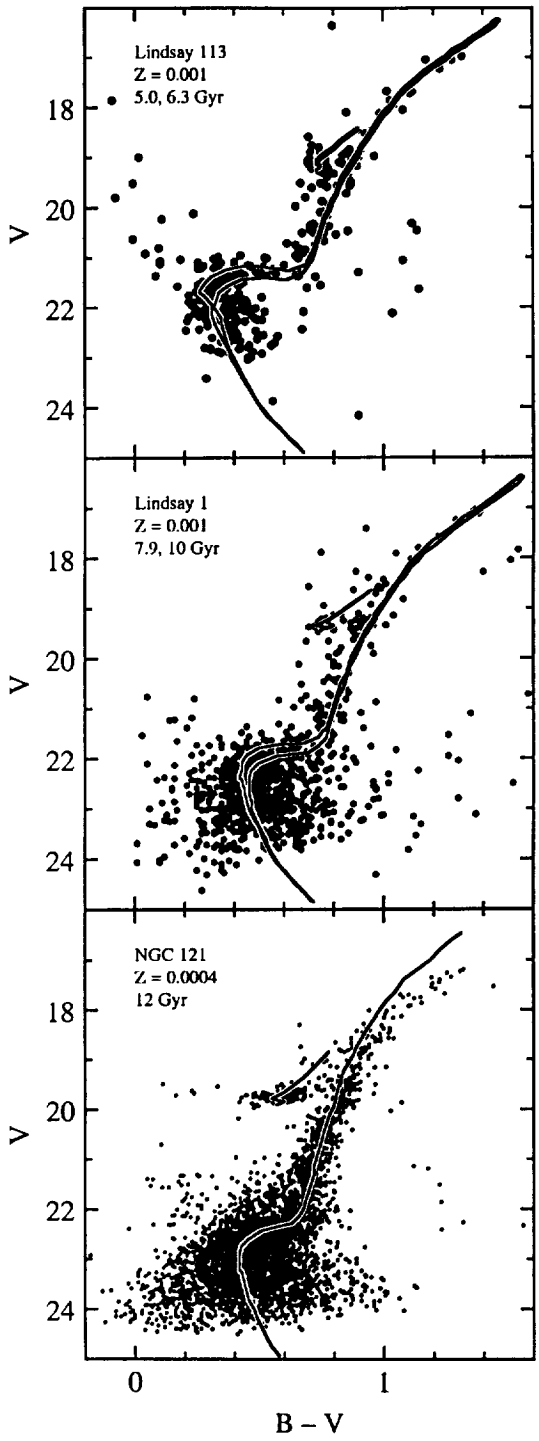

Fig. 9.— The V vs $B-V$ color-magnitude diagrams of the SMC populous clusters Lindsay 113, Lindsay 1, and NGC 121 (from top to bottom in order of increasing age and decreasing metallicity). Bertelli *et al.* (1994) theoretical isochrones for the indicated ages and metallicities are shown for comparision.

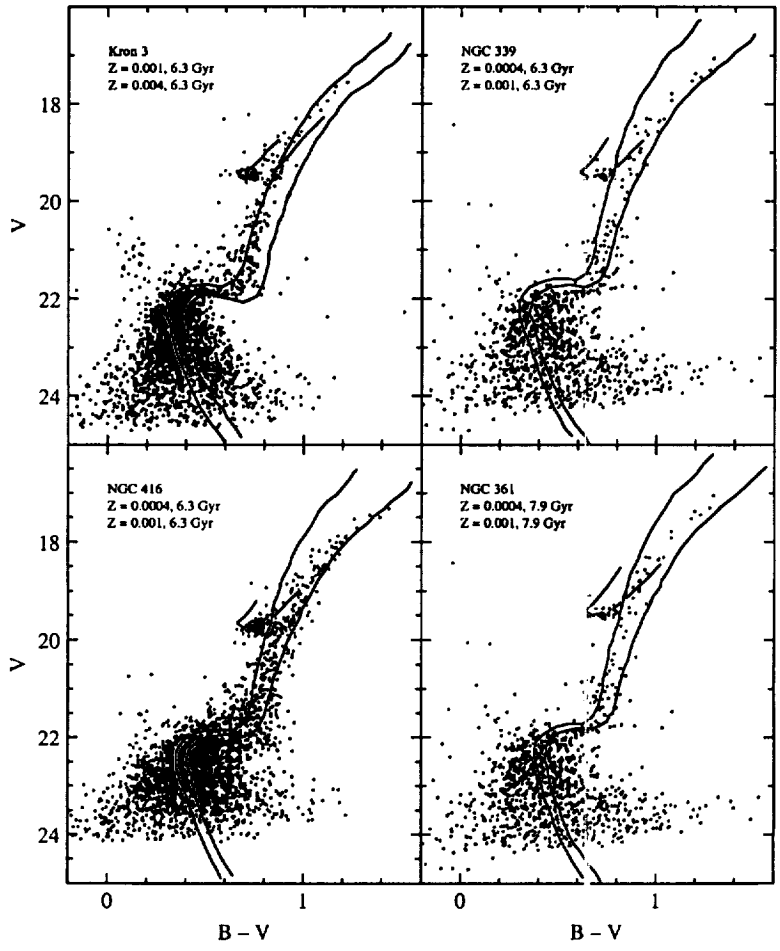

Fig. 10.— The V vs $B-V$ color-magnitude diagrams of the SMC populous clusters Kron 3, NGC 339, NGC 416, and NGC 361 (increasing age and decreasing metallicity from left to right and top to bottom). Bertelli *et al.* (1994) theoretical isochrones for the indicated ages and metallicities are shown for comparision.

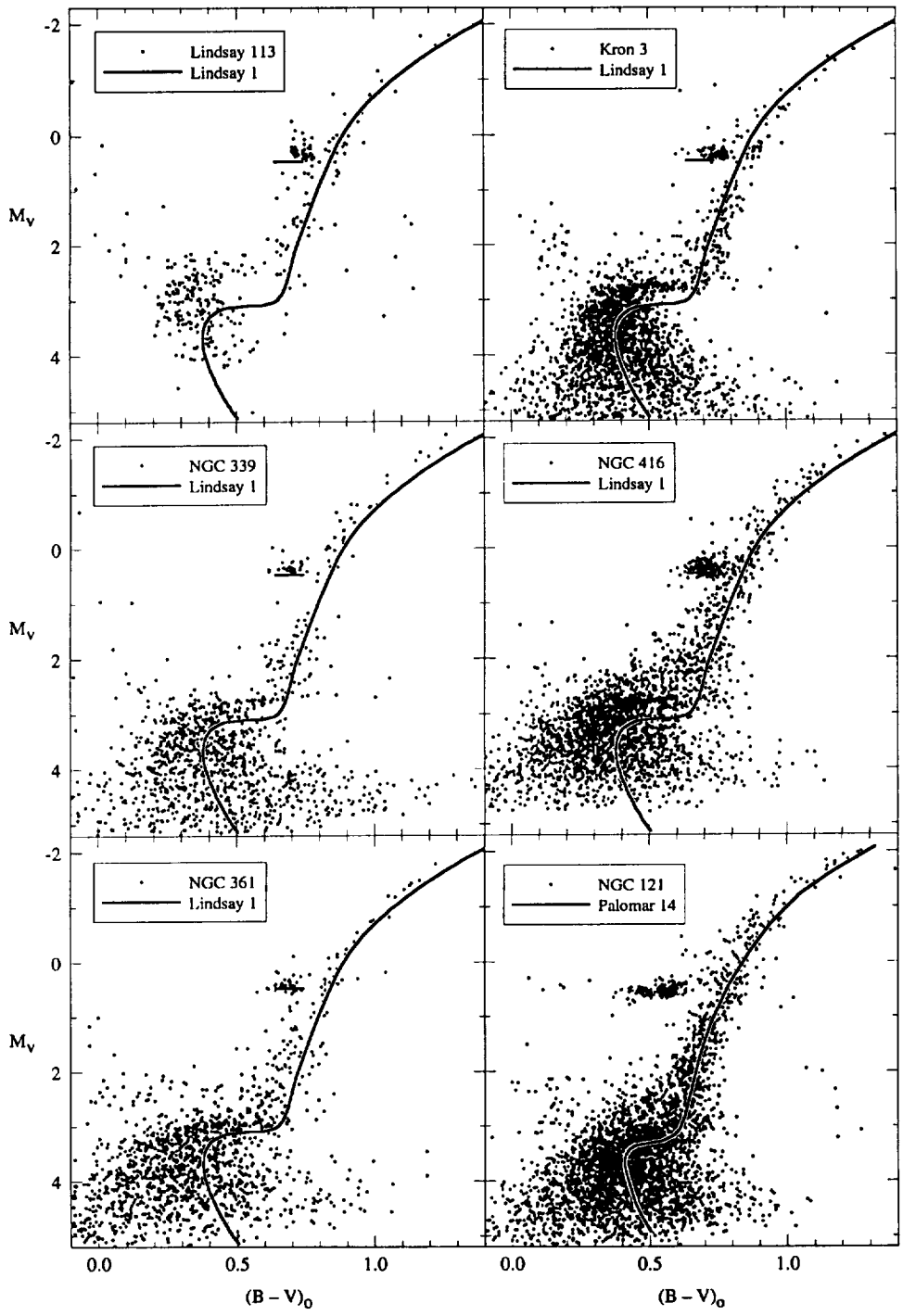

Fig. 11.— The M_V vs $(B-V)_o$ color-magnitude diagrams of the intermediate-age Small Magellanic Cloud populous clusters compared with the fiducial sequences for Lindsay 1 ([Fe/H] = −1.35) and Palomar 14 ([Fe/H] = −1.6). The clusters are plotted (top to bottom, left to right) in order of increasing age (see Table 9). We have used the Lindsay 1 fiducial derived from the photometry of Olszewski *et al.* (1987), the transformed *BV* Lindsay 113 photometry of PAPERI which was derived from the *BR* photometry of Mould *et al.* (1984), and the Palomar 14 fiducial derived from the photometry of Sarajedini (1997).

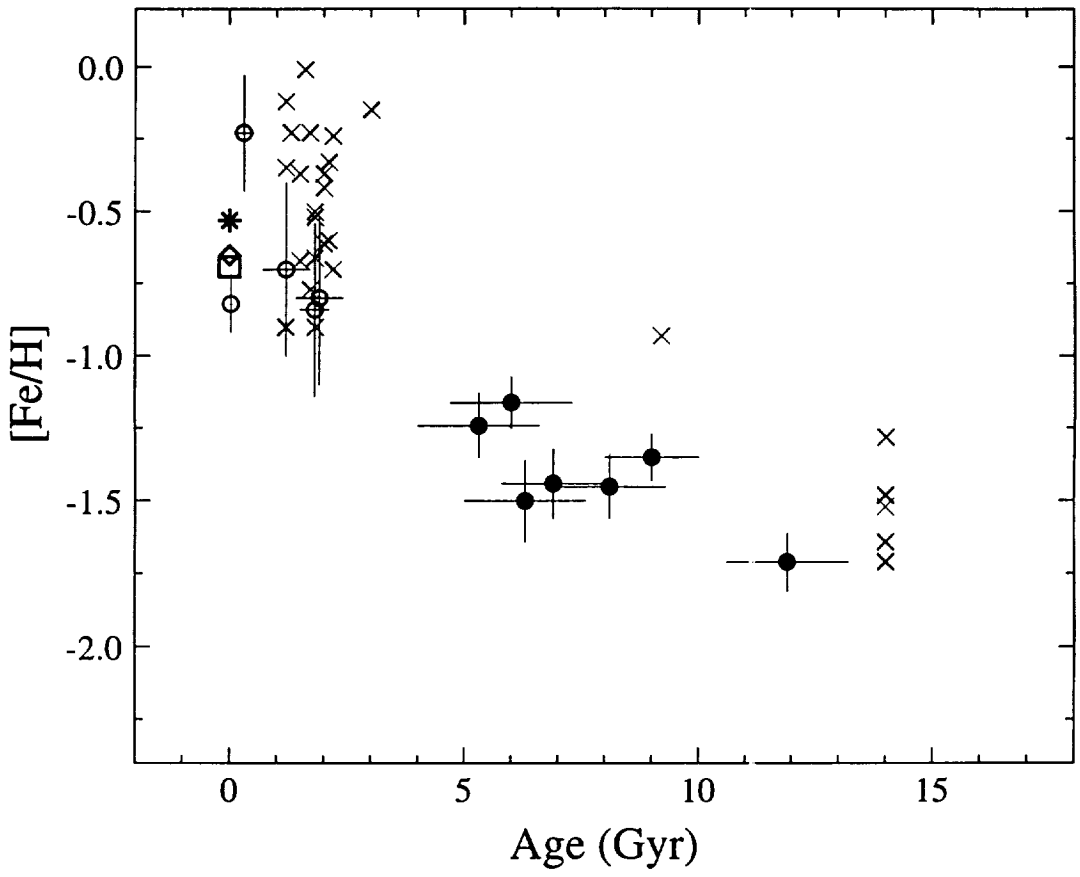

Fig. 12.— A plot of [Fe/H] vs age for Magellanic Cloud star clusters with precise metallicity and age determinations. Our estimates (**filled circles**) for Lindsay 113, Kron 3, NGC 339, NGC 416, NGC 361, Lindsay 1, NGC 121 (in order of increasing age) are combined with other SMC cluster data (**open circles**) from Da Costa & Hatzidimitriou (1998) The points marked as × are LMC clusters; the data for the oldest clusters are from Olsen *et al.* (1998) and the data for clusters younger than 10 Gyr are from Geisler *et al.* (1997) and Bica *et al.* (1998). The remaining three points are the present-day abundance of the SMC taken from Luck & Lambert (1992: **asterisk**), Russell & Bessell (1989: **diamond**), and Hill (1997: **square**). The errorbars reflect our estimates of the uncertainties in [Fe/H] and age.

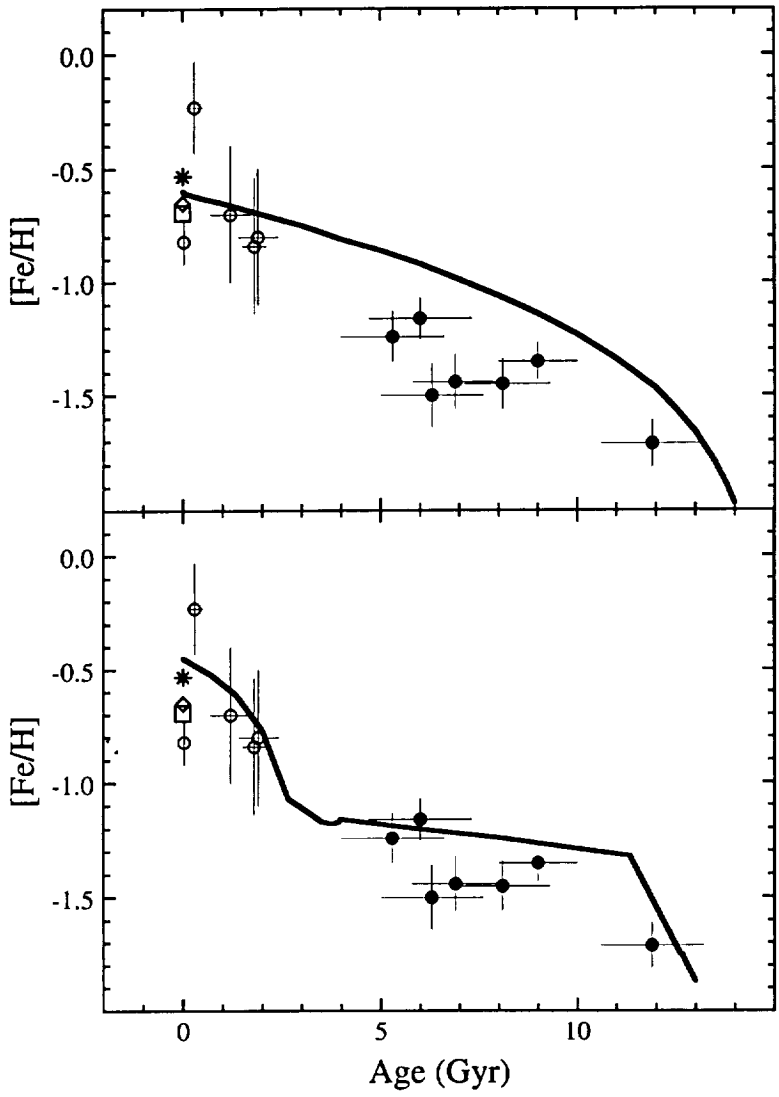

Fig. 13.— **Upper panel:** The age-abundance data for the 7 clusters discussed in this paper (**filled circles**) is compared with the closed box continuous star-formation model (**solid curve**) computed by Da Costa & Hatzidimitriou (1998, private communication) for an assumed present day metallicity of −0.6 dex for the SMC. The younger SMC cluster data (open circles) is from Da Costa & Hatzidimitriou (1998). The remaining three points are the present-day abundance of the SMC taken from Luck & Lambert (1992: asterisk), Russell & Bessell (1989: diamond), and Hill (1997: square). The errorbars reflect our estimates of the uncertainties in [Fe/H] and age. **Lower panel:** This panel is identical with the upper one except that the SMC bursting model (**solid curve**) of Pagel & Tautvaišienė (1998) is depicted.

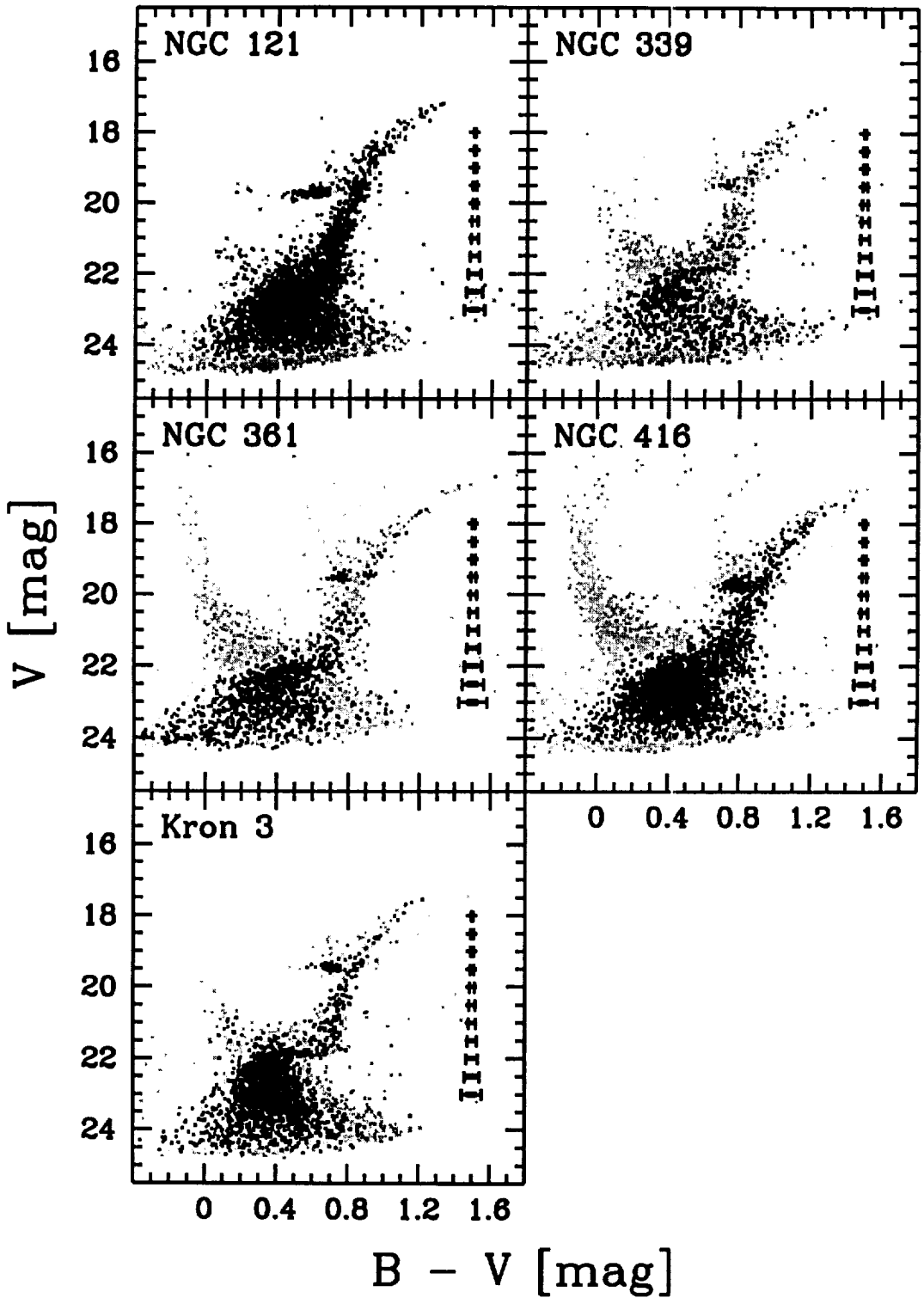

Fig. 14.— The V vs $B-V$ color-magnitude diagrams for the *HST* observations of the SMC populous clusters discussed in this paper. The total WFPC2 exposure times were $\lesssim$15 min; total spacecraft time for these *HST* observations was $\lesssim$27 min per cluster. The black dots are probable cluster members found on the PC1 CCD and the gray dots are stars found on the WF CCDs.